Effect of a Novel Dowel and Cramp On In-Plane Behavior of Multi-Leaf Stone Masonry Walls Proposed for Modern Masonry Buildings

Ahmad Javid Zia * and Abdulkerim İLGÜN

Posted Date: 17 April 2023

doi: 10.20944/preprints202304.0444.v1

Keywords: Dowels and cramps; Diagonal compression test; Multi-leaf stone wall; shear test; Compression test

Article

Effect of a Novel Dowel and Cramp on In-Plane Behavior of Multi-Leaf Stone Masonry Walls Proposed for Modern Masonry Buildings

Ahmad Javid Zia [1,*] and Abdulkerim İlgün [2]

[1] KTO Karatay University, Faculty of Engineering and Natural Sciences, Civil Engineering Department, javid.zia@karatay.edu.tr
[2] KTO Karatay University, Faculty of Engineering and Natural Sciences, Civil Engineering Department, kerim.ilgun@karatay.edu.tr
* Correspondence: javid.zia@karatay.edu.tr

Abstract: This study discusses the experimental assessment of the in-plane mechanical behavior of a multi-leaf stone masonry wall built from cut stone and reinforced with metal connectors (cramps and dowels). The wall, inspired by conventional multi-leaf stone walls, is meant for use in modern stone masonry buildings. The wall is constructed from two parallel load-bearing walls with a cavity between them, which aims to conceal the installation and insulation needed in modern buildings. The load-bearing walls are connected with cramps and dowels at certain intervals so that the wall works as a single section against horizontal and vertical loads. To characterize the in-plane behavior of the proposed wall, compressive, triplet, and diagonal compression tests were conducted to investigate the compressive strength, shear strength, modulus of elasticity, stiffness, ductility, and energy absorption of the wall. Compared with dry and mortar joint walls, the use of dowels increased the initial shear capacity of the wall by 11 and 19 times, respectively. The application of cramps without curving channels inside the individual stone elements decreased the compressive strength by 18%. The energy absorption of the designed walls with metal connectors was substantially increased to that of the specimens representing conventional stone walls. The results obtained show the applicability of the wall due to its higher shear strength and minimal drop in compressive strength, which is within acceptable limits.

Keywords: dowels and cramps; diagonal compression test; multi-leaf stone wall; shear test; compression test

1. Introduction

Today, in many parts of the world, the remains of complex buildings demonstrating a high degree of engineering skills in masonry construction rather than rudimentary shelters can be found. Most of these buildings are composed of stone, which is a brittle and heavy material used for construction [1]. Constructing such buildings has never been an easy task. Factors such as the low tensile strength, heavy mass, and brittle characteristics of the stone and, most importantly, the vulnerability of stone-made buildings to higher earthquake loads, especially due to the increased total weight of the building, serve as considerable challenges. Through the years, these challenges were obviated with innovative ideas such as using arches, domes, and multi-leaf walls as well as strengthening ashlar masonry with dowels and cramps using different materials [2]. Due to the abovementioned factors, ancient buildings, which have survived severe earthquakes and destructive environmental effects over many years, are the most precious inheritance for the countries they exist in today.

In our era, buildings can be built to be more durable at fair prices due to the characteristic features of materials such as steel, concrete, and other composites used in the building sector. On the other hand, the use of natural materials, such as stone, in load barrier elements has been marginalized and pushed aside. This is because stone-made load barrier elements, such as stone masonry walls, exhibit brittle behavior due to rapid loss of stiffness, strength, and energy absorption [3]. Natural

materials like stone are only utilized as coatings in the construction of modern buildings. Despite the availability of modern materials, a structure made of natural materials such as stone, designed to be earthquake resistant with innovative engineering solutions, remains a covetable and invaluable masterpiece.

In the literature, many valuable studies are devoted to characterizing masonry structures' behaviors. Nonetheless, strengthening historical masonry buildings is generally at the forefront [4]. For instance, Abdulsalam et al. [5], Anglad et al. [6], and other researchers [7–9] investigated the retrofitting of historical masonry buildings with modern construction materials. Hereupon, several reviews devoted to a specific aspect, e.g., characterizing the mechanical behaviors of the materials used in the masonry wall [10–14], characterizing the mechanical behavior of masonry walls [15–21] or modeling, improving and, evaluating the seismic performance of the historical stone masonry buildings [22–27]. However, to the best of our knowledge, most studies have been carried out because of the need to conserve historic buildings. Moreover, none of them have proposed a masonry wall type that can be used in the construction of new modern masonry buildings, which will provide the majestic appearance of stone masonry buildings while being more durable than those constructed with the currently used methods and building materials.

For this reason, in this study, a newly designed natural stone masonry wall to be used for modern buildings is proposed. The proposed wall consists of two layers and a cavity between them. The layers of the wall are connected with metal connectors (cramp and dowel) designed in this study. The aim is to conceal all necessary installments inside the cavity of the wall and improve the mechanical properties of the wall against in-plane and out-of-plane loads by combining two layers into one. The design principle of the proposed wall is based on meeting the needs of a modern building without vitiating the appearance of the stone wall while being more durable against earthquakes.

The study represents the experimental assessment of the in-plane mechanical behaviors of the proposed wall. It consists of two main parts. In the first part, the application of the proposed multi-leaf (cavity wall) stone masonry wall is designed. In the second part, a series of experimental studies were carried out. The experimental studies consist of determining metal connectors design parameters, characterizing the mechanical properties of the material used in the wall, characterizing the compressive and shear strength of the wall as well as determining Young's modulus, stiffness, ductility, and energy absorption of the proposed wall. The shear strength, stiffness, and ductility of the wall were characterized by the shear test method complied with the initial shear test methodology described in EN 1052-3 [28] and Diagonal Compression Test (DCT) described in ASTM E 519M-15 [29]. The compressive strength and Young's modulus of the proposed wall were determined by the compression test complied with the test methodology described in EN 1052-1:1999 [30].

In summary, the novelty of this paper is to experimentally determine the mechanical properties of a newly designed stone multi-leaf (cavity wall) wall. This wall is meant to be used in constructing new modern masonry buildings with majestic architecture thereby providing all the comforts of a modern building along with durability. In addition, paving the way for further investigation of the in-plane behavior under cyclic-loads, out-of-plane mechanical behaviors and the carbon footprint of the proposed wall.

2. Materials and Methods

2.1. Proposed wall

The proposed wall was inspired by conventional multi-leaf stone masonry walls, such as those described in [10,20,31–37], with a change in its load transfer mechanism. The wall consists of two load-bearing walls (each one is called a layer) and a cavity between them, as shown in Figure 1. Due to the cavity between these two load-bearing walls, it looks the same as sandwich or cavity walls [38–43]; however, the proposed wall is constructed with naturally cut stone and reinforced with cramps and dowels, which are designed to enhance the in-plane and out-of-plane mechanical behavior of the wall. Conventional cavity walls are usually built from brick or concrete blocks, and one of the two

Preprints (www.preprints.org) | NOT PEER-REVIEWED | Posted: 17 April 2023 doi:10.20944/preprints202304.0444.v1

parallel walls is load bearing, where the second wall is usually for cladding. In the proposed wall, both layers are built from cut stone and act as load-bearing elements.

In the proposed wall, the two parallel layers and all individual stones in each layer are tied to each other with metal cramps and dowels (Figure 1). Thus, by connecting two parallel walls, they will operate as a single section, and the in-plane and out-of-plane behaviors of the wall are strengthened with metal connectors. The cavity between these two layers is of paramount importance. First, it is designed to insulate and conceal all installations needed in the building without vitiating the majestic appearance of the stone wall in the building. In addition, omitting the middle layer, as it is an important part of conventional multi-leaf stone walls, decreases the total weight of the building, which results in reduced earthquake loads. Moreover, the low mechanical strength and the flaws in the application of the middle layer in conventional multi-leaf stone walls are generally inadequate for maintaining the connection of the two outer layers under in-plane and out-of-plane loads. Therefore, the failure in conventional multi-leaf stone walls is brittle [33,44], which is generally not acceptable by any building code and regulations. As in the proposed multi-leaf stone masonry wall, the two outer layers are connected with cramps and dowels to assure that the wall works as a single wall (Figure 1).

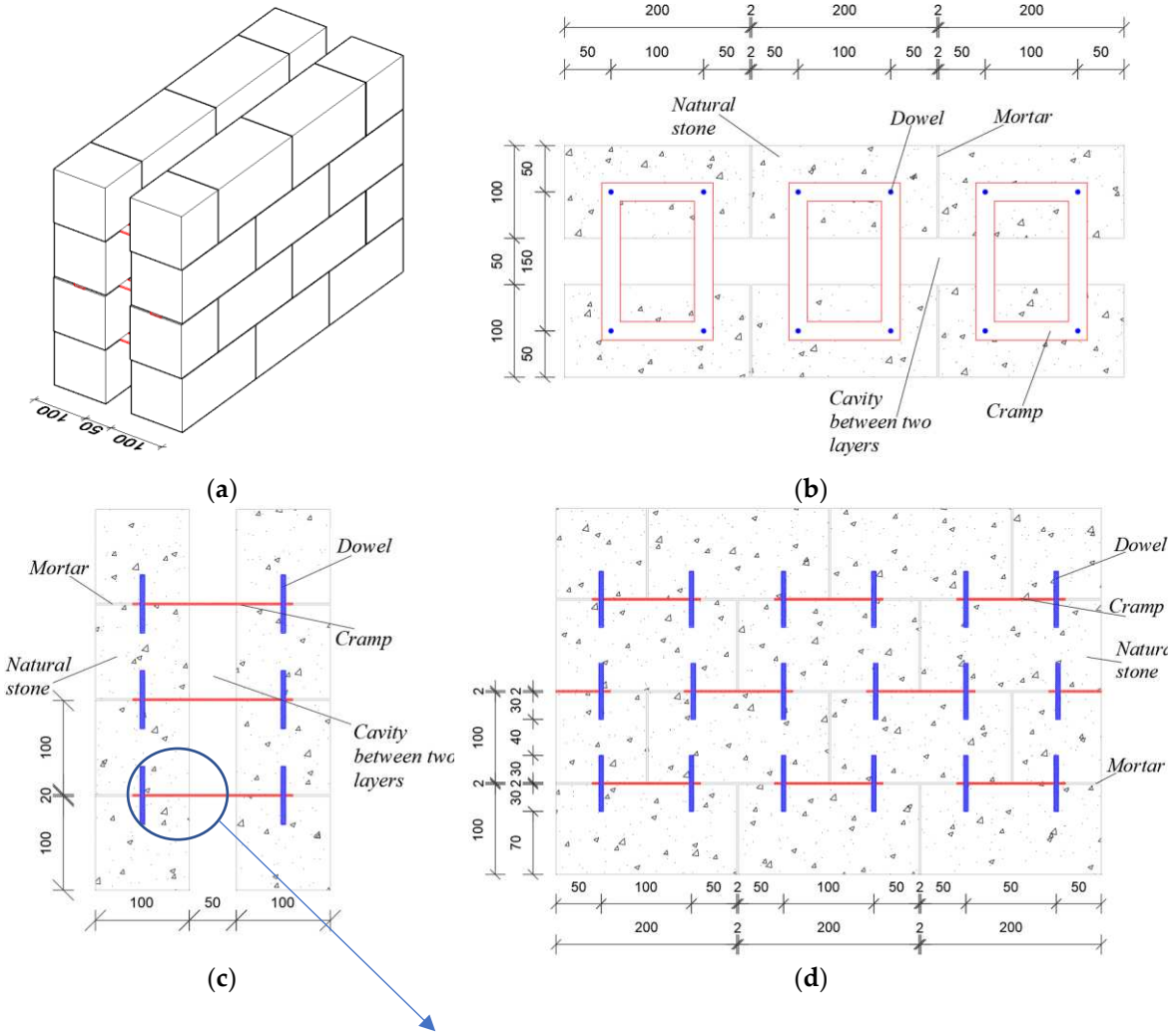

Preprints (www.preprints.org) | NOT PEER-REVIEWED | Posted: 17 April 2023 doi:10.20944/preprints202304.0444.v1

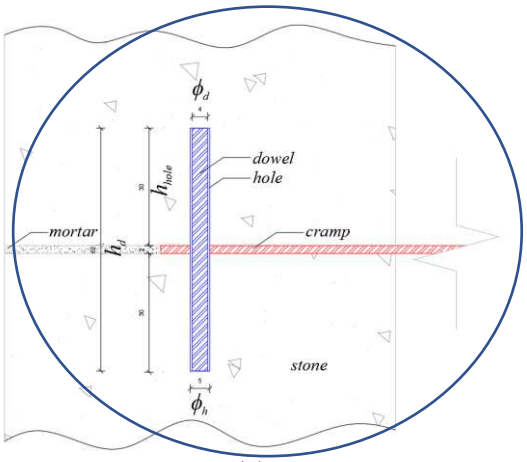

(e)

Figure 1. Details of the proposed multi-leaf wall (mm): (**a**) Perspective view; (b) Plane view (3rd row); (**c**) Wall cross-section; (**d**) Surface cross-section; (**e**) Application of cramp and dowel between two vertical stones.

The application of the proposed wall can be broken into 4 stages which are shown in Figure 2.

Stage 1: The foundation stone, which has a width equal to the width of the proposed wall (the total thickness of two layers + cavity), is applied on the reinforced concrete foundation, connecting the two layers of the proposed wall.

Stage 2: only one layer (preferably the outer layer) of the wall with U-type cramps and dowels is built (Figure 2 – Stage 1-2).

Stage 3: After the completion of one layer, the insulation, and installations needed in the building are applied (Figure 2 – Stage 3).

Stage 4: The second layer with U-type cramps is built, and the U-type cramps are connected via pins (Figure 2 – Stage 4). In this way, all of the necessary installations in a building will be hidden inside the wall, and the appearance of the stone wall will not be damaged (Figure 2 – Finale stage).

(a)

(b)

(c)

(d)

Preprints (www.preprints.org) | NOT PEER-REVIEWED | Posted: 17 April 2023 doi:10.20944/preprints202304.0444.v1

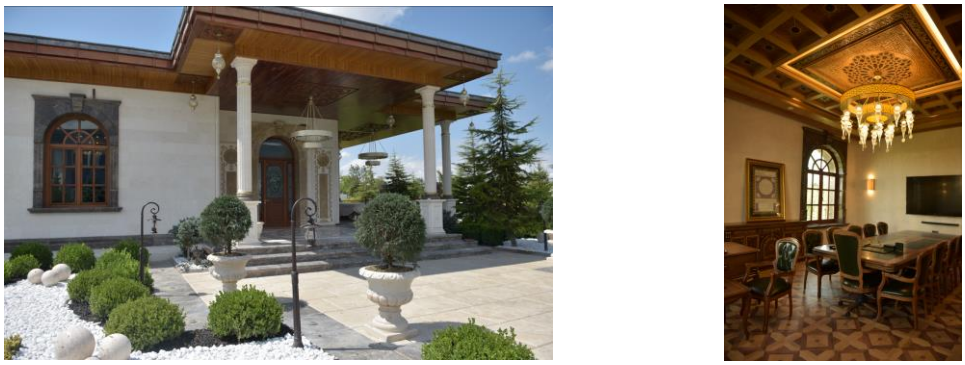

(**e**) (**f**)

Figure 2. Stages of the proposed wall's application in a model stone masonry building built in Konya - Turkey: (**a**) Stage 1: Application of foundation stone under the wall; (**b**) Stage 2: Build one layer of the wall with U-type cramps and reinforcing with dowels; (**c**) Stage 3: Finishing only one layer of the wall and applying the insulation and installations; (**d**) Stage 4: Building the second layer with U-type cramps and connecting two cramps; (**e**) Final stage: The exterior of the building built with a proposed multi-leaf stone wall; (**f**) Final stage: The interior of the building built with the proposed multi-leaf stone wall.

In this study, as there was no insulation or installation, the cramps were prepared as rectangular elements rather than U-type elements, as shown in Figure 3. In the proposed wall, for a single leaf, individual stones are connected via mortar and metal connectors. First, proper holes (1 mm larger than the diameter of the dowels) are drilled into each stone. Then, after placing two individual stones side by side, metal connectors (cramps and dowels) are applied, and the remaining part around the cramps is filled with mortar with a thickness equal to the cramp thickness. It should be noted that the holes drilled for dowels are not filled with mortar or any other material. For multi-leaf walls, the construction phase is the same as that of a single-leaf wall. The only difference is the connection of two layers with metal connectors, which are designed to ensure the integrity of the wall.

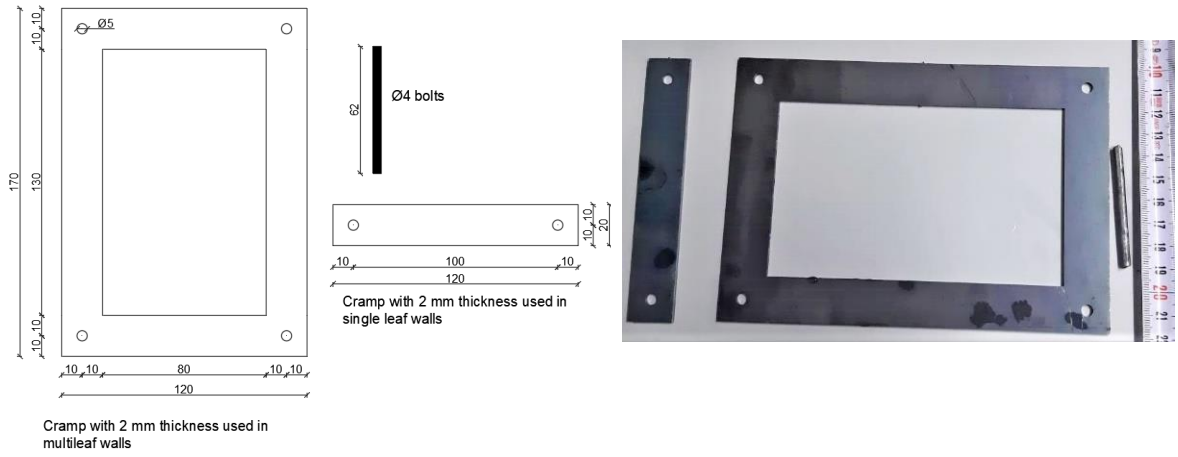

Figure 3. Details of cramps used in single- and multi-leaf walls (units are in mm).

2.2. Properties of materials

The mechanical properties of the materials used in the experimental work are shown in Table 1. The stone used in this study is called Myra Beige, which is a natural limestone found in Turkey. The compressive strength of the stone, obtained from a uniaxial compression test following EN 1926 [45], is the mean value of 30 specimens with a size of 50 × 50 × 50 mm. The tensile strength of the stone is the mean value of 20 specimens with a size of 50 × 50 × 300 mm, and appropriate tests were carried out following EN 12372 [46]. Young's modulus of the stone was obtained from 6 specimens with a size of 50 × 100 × 200 mm tested according to EN 14580 [47].

Preprints (www.preprints.org) | NOT PEER-REVIEWED | Posted: 17 April 2023 doi:10.20944/preprints202304.0444.v1

Table 1. Average mechanical properties of the materials used in the experimental program.

Material	f_i (N/mm²)	f_{tc} (N/mm²)	F_y (N/mm²)	F_u (N/mm²)	E (GPa)	F_τ (N/mm²)
Stone	50	12.2	-	-	15	-
Mortar	1.46	0	-	-	-	-
Cramps	-	-	227	330	114	-
Dowels	-		-	61	602	31

f_i: compressive strength; f_{tc}: tensile strength; F_y: yield strength; F_u: ultimate strength; E: Young's modulus; F_τ: shear strength .

The lime mortar used in this study was produced from a mixture determined after a brief literature review [48–50]. The binder/aggregate ratio was selected as 1:3, and hydrated lime was used as the binder. River sand, white sand, and marble powder were used as aggregates at a ratio of 3:2:1. All aggregates were sieved through a sieve with a 2 mm hole diameter. The compressive and tensile strengths of the mortar were determined at 28 days. As observed, the mechanical strength of lime mortar at this age is very low. Nevertheless, in all test specimens, this mortar was used. The thickness of the head and bed joints in the test specimens was cast as 2 mm, which is equal to the thickness of the metal cramps used in the bed joints. Accordingly, as in the case of compression, the uniaxial load is transferred from stone to stone through cramps, which has a higher mechanical property than the mortar used. Mortar is only used as a bonding material, not as a load-transferring element. Therefore, the poor mechanical properties of mortar should not have any effect on the mechanical characterization of the proposed wall. The only problem that may arise with low-strength mortar is the formation of cracks in the mortar, which would ease moisture penetration. To preserve the metal connectors from rust in new modern masonry buildings, all metal elements are galvanized before application. Nevertheless, the tensile and compressive strengths of the mortar were determined from the data of 3 specimens tested following EN 1015-11 [51].

The mechanical properties of metal connectors, which consist of cramps and dowels, were determined by the TS EN ISO 6892-1 standard [52]. Cramps are made from S235JR steel, which is a soft structural steel that can be easily welded and bent. For dowels, because of the small diameters (4 mm, 5 mm, and 6 mm) required for this study, steel mesh or wire mesh was acquired and used. Young's modulus of the cramps was easily calculated from the stress–strain curve due to the obvious yield stress, but for the dowels, the yield strength was ambiguous. Therefore, Young's modulus was determined from the stress corresponding to 0.002 strain. The yield strength (F_y), ultimate strength (F_u), and Young's modulus (E) of the cramps and dowels were the mean values of 5 and 8 specimens, respectively (Table 1). Among the 8 dowel specimens prepared for the tensile test, there were 3 specimens with a 4 mm diameter, 3 specimens with a 5 mm diameter, and 2 specimens with a 6 mm diameter.

In addition to the tensile strength of the dowels, a proper shear test was carried out to characterize the shear (cutoff) strength of the dowels. The details of the shear test setup are shown in Figure 4, and the mean value of the shear strength (F_τ), which was calculated from 6 specimens with two different diameters (4 and 5 mm), is given in Table 1.

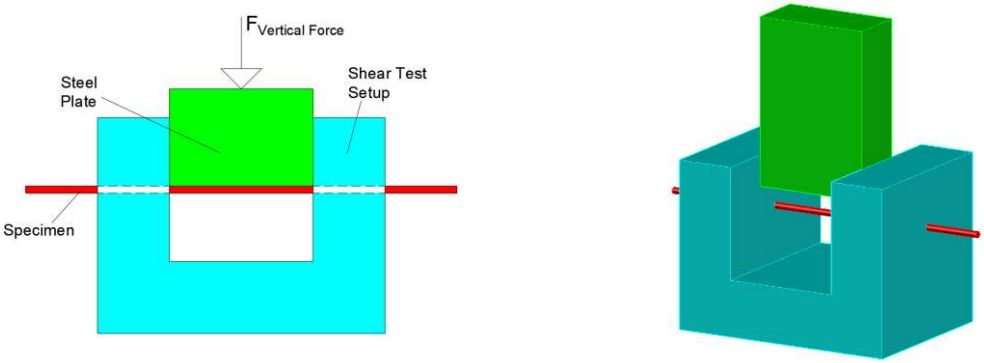

Figure 4. Details of the shear test setup designed for the dowels (mm).

2.3. Experimental Program

The experimental program in this study consists of determining the optimum diameter for dowels and characterizing the effect of metal connectors (cramps and dowels) on the in-plane behavior of the proposed multi-leaf stone masonry walls by evaluating the shear and compressive strength, modulus of elasticity, stiffness, ductility, and energy absorption of the proposed walls. In all test specimens, the individual stone sizes were used as 100 × 200 × 100 mm (full stone) and 100 × 100 × 100 mm (half stone) (width × length × height).

2.3.1. Metal connectors

Information regarding cramps is limited in the literature [10]. Therefore, the width of the cramps was selected to be 20 mm, according to [53], and the thickness of the cramps was selected as the joint thickness, which was 2 mm. These two parameters can be optimized. However, in this study, the out-of-plane behavior of the proposed wall was not investigated because out-of-plane studies need a thorough experimental campaign [8,38,54–56]; hence, the abovementioned dimensions were utilized. The length of the dowels was selected as 62 mm, which according to [57] has a small effect on the shear strength. The most important parameter in this study was to find the optimum dowel diameter. For this purpose, a series of triplet tests were performed on specimens with dry joints, which were reinforced with proposed metal connectors (cramps and dowels); these tests were performed with different dowels diameters following EN 1052-3 [28]. As reported in [57], compared with thinner dowels, thicker dowels give a higher shear bearing capacity and provide higher stiffness, which implies lower displacements. Following this, thicker dowels would be preferable to increase the shear capacity of the stone walls. However, it should be noted that thicker dowels may result in a higher shear capacity of dowels, thereby breaking the stone units before the dowel's cutoff. This may result in the failure of the wall under both compression and shear. In other words, for the proposed wall under shear stress, dowels are preferred to be the weak link in the chain rather than the load-bearing individual such as the stone. Therefore, a series of triplet tests were carried out with different dowel diameters (3, 4, 5, and 6 mm) to ascertain the optimum dowel size, which results in dowel cutoff before individual stone failure. In addition, the effect of cramp application on the compressive behavior of the wall was also investigated with a simple compression test carried out on 10 specimens, whose details are given in section 3.1.

2.3.2. Test specimens

Apart from 46 specimens built for pre-experimental work to determine the optimum dowel diameter and cramp effect on the compression tests, a total of 61 specimens were constructed for the experimental study, 48 of which were built in a micro-size and the remaining 13 in a macro-size. Out of the total 48 specimens, 12 were built for the compressive test and the remaining 36 were used to determine the initial shear strength. As for macro-sized specimens, 4 were built for the compressive test and 9 were built for the diagonal compression test.

- Micro-sized specimens

To quantify the compressive strength of the proposed wall in accordance with EN 1052-1:1999 [30], 12 micro-sized specimens were built. These specimens were divided into 4 groups, whose detailed information is given in Table 2. The first group contains 3 single layer of dry joint specimens, in which individual stones were placed upon each other without any mortar or metal connectors. The specimens in the second group were built as a single layer, and the individual stones were joined only by 2 mm mortar. These 3 specimens were evaluated as a reference to see the effect of metal connectors in the proposed walls. The third group contains specimens of the same size as the specimens in the second group, but individual stones were connected with metal connectors (cramp and dowel) in addition to the mortar (Figure 5. a). The metal connectors used in this group consisted of cramps and dowels with the dimensions given in Figure 3. The last group contains 3 specimens

Preprints (www.preprints.org) | NOT PEER-REVIEWED | Posted: 17 April 2023 doi:10.20944/preprints202304.0444.v1

that represent the proposed walls, which were made of two layers with a 50 mm cavity between them. Both layers were joined by cramps and dowels designed in this study (Figure 5. b and c).

As in the compression test, the micro-sized specimens in the shear test also consist of 4 types of wall specimens. The first type was a single-layer wall with dry joints. The second type was a single-layer wall with only 2 mm mortar joints. The third type consisted of single-layer walls with joints containing mortar and metal connectors (Figure 5.d). Finally, the fourth type refers to specimens built as multi-leaf walls with a cavity between the two layers and connected with metal connectors (Figure 5. e and f). Detailed information is given in Table 2.

Table 2. Detailed information regarding micro-sized compressive and shear test specimens.

Code name	Test Setup	Number of layers	Metal connectors	Mortar	Number of specimens	Specimen size (mm) (width×length×height)
SWC	Compression	Single	No	No	3	100 × 400 × 500
SWLC	Compression	Single	No	Yes	3	100 × 402 × 508
SWMLC	Compression	Single	Yes	Yes	3	100 × 402 × 508
DWMLC	Compression	Double	Yes	Yes	3	200 × 402 × 508
SWIS	Initial Shear	Single	No	No	9	100 × 200 × 300
SWLIS	Initial Shear	Single	No	Yes	9	100 × 202 × 304
SWMLIS	Initial Shear	Single	Yes	Yes	9	100 × 202 × 304
DWMLIS	Initial Shear	Double	Yes	Yes	9	200 × 202 × 304

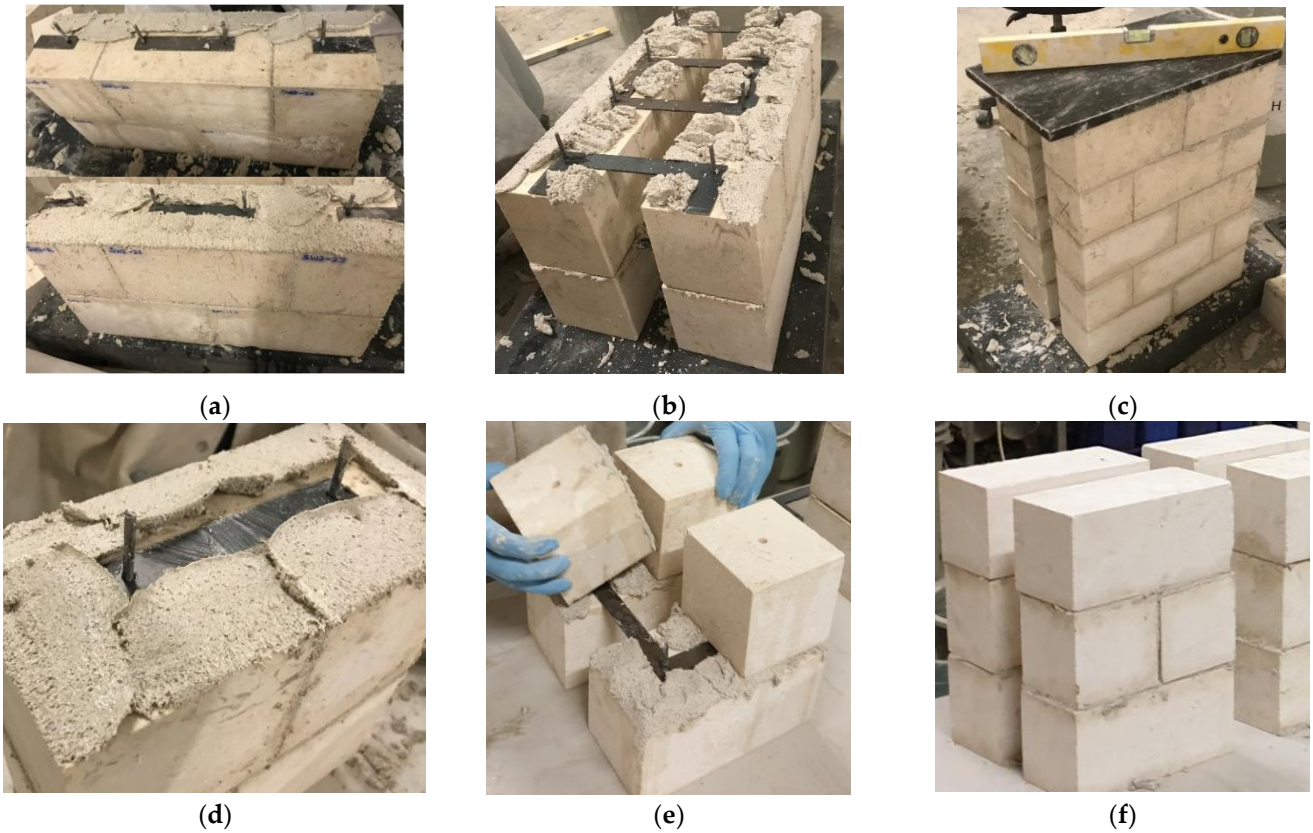

Figure 5. Details of micro-sized specimens for compression and initial shear test: (**a**) Single layer with lime mortar + metal connectors (compression); (**b**) Multi-leaf with lime mortar + metal connectors (compression); (**c**) The proposed multi-leaf wall (compression); (**d**) Single leaf with lime mortar + metal connectors (initial shear); (**e**) Multi-leaf with lime mortar + metal connectors (initial shear); (**f**) The proposed multi-leaf wall (initial shear).

- Macro-sized specimens

Preprints (www.preprints.org) | NOT PEER-REVIEWED | Posted: 17 April 2023 doi:10.20944/preprints202304.0444.v1

As stated in [58], the size of the specimen plays a crucial role in determining the stiffness, strength, and failure mechanism of masonry walls under experimental studies. Therefore, in addition to 48 micro-sized specimens, a total of 13 macro-sized specimens were built to characterize the compressive, shear strength, modulus of elasticity, stiffness, ductility, and energy absorption of the proposed wall. Of these 13 specimens, 4 were built for the compressive test and the remaining 9 for the diagonal compression test whose details are given in Table 3 and Figure 6.

The specimens prepared for the diagonal compression test were determined by the ASTM E 519M-15 [29] standard. However, no standard exists for macro-sized specimens built for compressive tests. Hence, there are many studies on characterizing masonry walls using macro-sized specimens in the literature [59–62]. The size of the macro specimens for compression tests was determined by considering the effect of the slenderness ratio of the wall used in the model stone building.

Types of macro-sized specimens were almost the same as micro-sized specimens. For the compressive test, 4 types of specimens were built. The first specimen type MSWC was built only by placing the stone on top of each other without any mortar or connectors. In the second specimen (MSWLC), the stones were connected only with lime mortar, and in the third specimen (MSWMLC), metal connectors were used in addition to lime mortar (Figure 6. a). The fourth type of specimen represents the proposed multi-leaf stone walls (Figure 6. b and c.). This sample, named MDWMLC, consists of two layers and there was a 50 mm cavity between the layers.

For the diagonal compression test, three types of specimens were built. The first wall type (SWDT) was built only by joining stones with 2 mm lime mortar. The second wall (SWMDT) consists of 2 mm lime mortar + metal connectors. The third type (DWMDT) represents the proposed wall which was built as two layer and a 50 mm cavity between them (Figure 6. e and e.).

Table 3. Detailed information regarding macro-sized compressive and shear test specimens.

Code name	Number of layers	Metal connectors	Mortar	Number of specimens	Specimen size (mm) (width×length×height)
MSWC	Single	No	No	1	100 × 800 × 1400
MSWLC	Single	No	Yes	1	100 × 806 × 1426
MSWMLC	Single	Yes	Yes	1	100 × 806 × 1426
MDWMLC	Double	Yes	Yes	1	200 × 806 × 1426
SWDT	Single	No	Yes	3	100 × 1210 × 1222
SWMDT	Single	Yes	Yes	3	100 × 1210 × 1222
DWMDT	Double	Yes	Yes	3	200 × 1210 × 1222

(**a**) (**b**)

Preprints (www.preprints.org) | NOT PEER-REVIEWED | Posted: 17 April 2023 doi:10.20944/preprints202304.0444.v1

(**d**) (**e**) (**c**)

Figure 6. Details of macro-sized specimens for compression and diagonal compression test: (**a**) Single layer with lime mortar + metal connectors (compression); (**b**) Multi-leaf with metal connectors (compression); (**c**) Multi-layer with metal connectors (compression); (**d**) Multi-leaf with lime mortar + metal connectors (diagonal compression); (**e**) Multi-leaf with metal connectors (diagonal compression).

2.3.3. Experimental setup

The experimental campaign in this study, includes uniaxial compression, triplet, and diagonal compression test. The uniaxial compression test was carried out on 16 specimens with two different sizes (macro and micro-sized).

Compression test

As parameters of the mechanical behavior and a basis for numerical analysis, determining the compressive strength and modulus of elasticity of the proposed wall is of great importance. Furthermore, the effect of cramp application on the compressive strength of the proposed walls needs to be specified. Therefore, to determine the abovementioned mechanical behavior compression tests were carried out on 12 micro-sized specimens according to EN 1052-1:1999 [30]. In addition, to investigate the slenderness ratio, failure mechanism, and strength reduction due to the specimen's size, an uniaxial compressive test was carried out on 4 macro-sized specimens.

The specimens were subjected to uniaxial loading by a hydraulic jack with a capacity of 3000 kN. No capping was used between the loading plates and specimens. The load was applied on both layers uniformly. To measure the displacement of the specimens tested under uniaxial loading, a total of 6 linear voltage displacement transducers (LVDTs) were used. Four LVDTs were placed at two faces of each specimen following EN 1052-1 and two between the base and top steel plates to measure the total change in height of the specimen, whose details are shown in Figure 7. a. The compressive strength and Young's modulus of the specimens were calculated by Equation 1.

$$f_i = F_{v,max}/A_i \quad \text{and} \quad E_i = F_{v,max}/3 \times \varepsilon \times A_i \tag{1}$$

where $F_{v,max}$ is the maximum uniaxial load, A_i is the loaded cross-section of the specimen, and $1/3\varepsilon$ is the strain of the specimen corresponding to one-third of the maximum uniaxial load. The loaded cross-section for single-leaf specimens was calculated as 100×400 mm^2, and for multi-leaf specimens, it was calculated as $2 \times 100 \times 400$ mm^2.

As for macro-sized specimens, the test setup is the same as micro-sized specimens. Instead of LVDTs, 4 string gauges were used to measure vertical displacements. The compressive strength and

Preprints (www.preprints.org) | NOT PEER-REVIEWED | Posted: 17 April 2023 doi:10.20944/preprints202304.0444.v1

Young's modulus of the specimens were calculated by Equation 1. The details of both macro and micro-sized specimen compression test setups are shown in Figure 7. a and b, respectively.

Triplet test

To quantify the shear strength of the proposed multi-leaf stone masonry wall, a triplet test was carried out on 36 specimens following EN 1052-3 [28]. The application of the triplet shear test setup proposed by EN 1052-3 (Figure 7. e) could not be adopted in this research due to the fragility of specimens with 2 mm mortar joints, especially during transfer and placement inside the test setup. Therefore, the test setup was modified as shown in Figure 7.d, keeping the logic of the shear test setup proposed by the EN 1052-3 standard.

Following EN 1052-3, all specimens were first subjected to a certain vertical pre-compressive load, and then a horizontal load was applied to the middle stone row until failure occurred. The failure of the specimen was accepted as the sliding of the middle (2nd) row occurred and the horizontal load took almost a constant value. The movements of the upper and lower rows (1st and 3rd rows) were prevented by rigid supporters. The magnitudes of vertical loads were applied following EN 1052-3, which were calculated in the form of stress as 0.2 MPa, 0.6 MPa, and 1 MPa. To keep the vertical loads constant, the horizontal friction force between the test setup and the specimen was abated by placing steel plates at the top and bottom of the specimen over steel rollers (Figure 7. c and f). The displacements of all stone layers were measured and recorded by LVDTs (Figure 7. c and f).

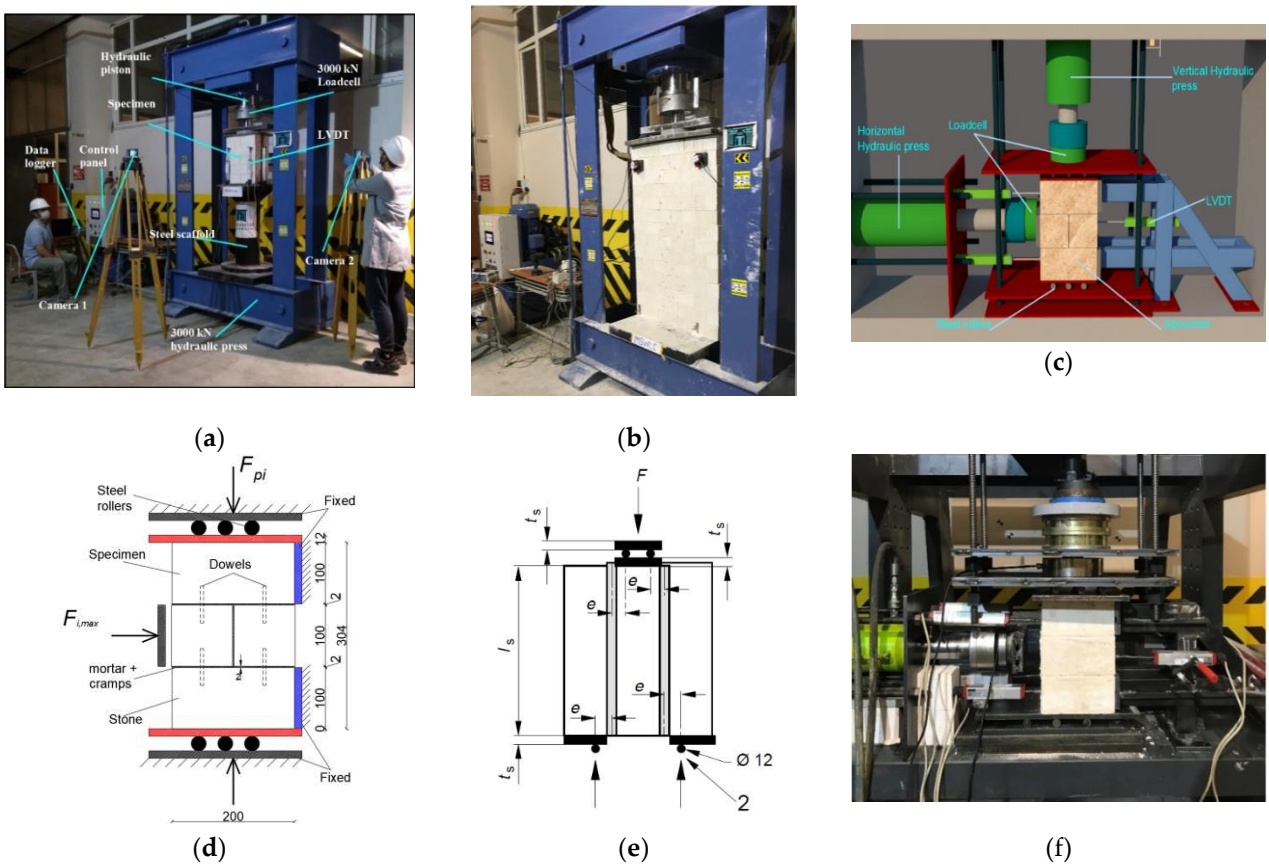

Figure 7. Details of compression and triplet test setups: (**a**) Micro-sized compression test setup; (**b**) Macro-sized compression test setup; (**c**) Schematic details of the initial shear test setup; (**d**) Test setup modified and used in this research; (**e**) Test setup proposed by the EN 1052-3 standard; (**f**) Triplet shear test setup.

As given in EN 1052-3, the shear strength f_{voi} and pre-compression stress f_{pi} were calculated according to Equations 2 and 3 for each specimen, where $F_{i,max}$ is the maximum horizontal load, A_i is

Preprints (www.preprints.org) | NOT PEER-REVIEWED | Posted: 17 April 2023 doi:10.20944/preprints202304.0444.v1

the net shear cross-section (parallel to the horizontal load and bed joint) of the specimens and F_{pi} is the pre-compression force.

$$f_{voi} = F_{i,max}/2A_i = F_{i,max}/2b_i(l_i-\Delta l_i) \quad (2)$$

$$f_{pi} = F_{pi}/A_i \quad (3)$$

After determining the shear strength of every single specimen, a graph of the individual shear strength f_{voi} against the normal compressive stress f_{pi} was plotted. Then, a line determined from linear regression was plotted, and the initial shear strength f_{vo} at zero normal stress was obtained. According to EN 1052-3, the characteristic value of the initial shear strength can be calculated as f_{vok}, where $f_{vok} = 0.8f_{vo}$.

Diagonal compression test

In-plane shear strength of the multi-leaf stone wall proposed in this study was determined using the diagonal compression test method recommended by ASTM E 519M-15 [29]. The test specimens were built diagonally as seen in Figure 6. e. The special apparatus shown in Figure 8. b has been designed so that the wall specimens can be built diagonally and transported and placed in the experimental setup without causing any damage. This assembly consists of a platform with a V-loading head and two brackets. The V loading head on the platform has been prepared following ASTM E 519M-15 (Figure 8. a). The brackets were connected with L profiles (Figure 8. b and c.) during curing and transportation and were removed before the experiment started (Figure 8. d).

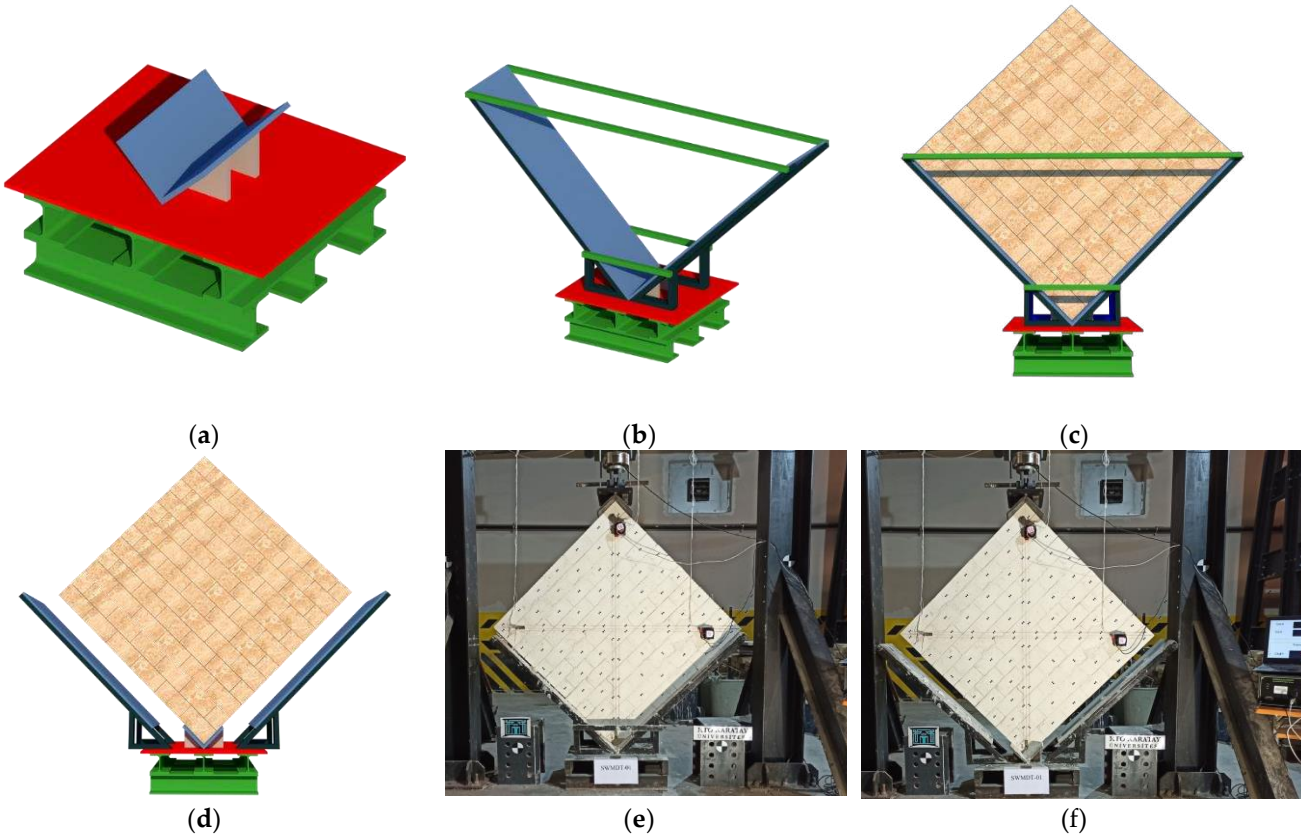

Figure 8. Diagonal specimen platform following ASTM E519: (**a**) V-head platform; (**b**) V-head Platform + wall brackets; (**c**) Wall specimen during curing and transport; (**d**) Wall specimen during the test; (**e**) Diagonal compression test setup (before the experiment starts); (**f**) Diagonal compression test setup (after the experiment starts).

As shown in Figure 8. e, a V-headed loading apparatus was placed at the upper end of the wall, and with the help of a 300 kN capacity hydraulic press, the brackets were removed by preloading

Preprints (www.preprints.org) | NOT PEER-REVIEWED | Posted: 17 April 2023 doi:10.20944/preprints202304.0444.v1

approximately 250 – 300 N, and the experiment was started. The brackets were first removed from the wall (Figure 8.d and f) and left leaning against the steel frame during the experiment to prevent the wall from collapsing rapidly and damaging the measuring instruments mounted on it, as shown in Figure 8. f.

3. Results

3.1. Optimum dowel diameter

To investigate the effect of dowel diameter on the proposed wall's shear strength, a triplet test was carried out following EN 1052-3 on 36 dry joint specimens with 4 different dowel diameters (3, 4, 5, and 6 mm). This test aimed to observe the shear failure mechanism. Two types of failure modes were observed during the conducted test. The first mode was elastic, followed by inelastic deformation in the dowels. This mode resulted in a dowel cut off at the surface of the stone, as shown in Figure 9. a. The second mode corresponded to the condition where both the shear and tensile capacities of the stone were exhausted before the maximum shear strength of the dowels. This mode resulted in the splitting of 100 × 100 × 100 mm^3 stones into two halves that were placed in the middle row (Figure 9. b).

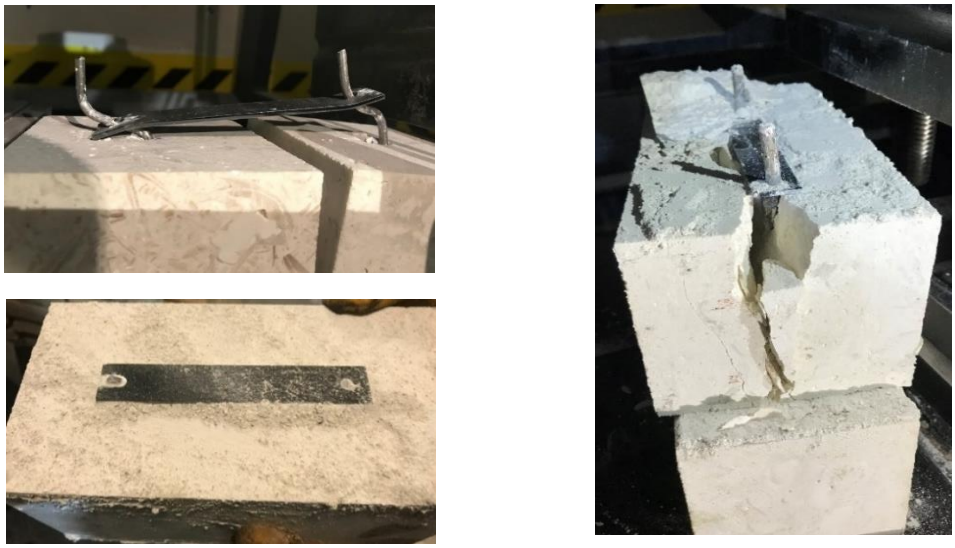

(**a**) (**b**)

Figure 9. Failure modes for determining the optimum dowel diameter: (**a**) Failure mode I; (**b**) Failure mode II.

The results of the triplet tests are given in Figure 10. c. Each bar represents the mean value of the three specimen results, and the horizontal red line roughly determines the boundary between mode I and mode II failure. As shown in Figure 10. d, two forces are exerted on the mentioned stone. The vertical load is applied as a tensile splitting force due to cramps, and the horizontal force acts as the shear force due to the dowels. In designing the optimum dowel diameter, these forces should be considered. Mode II occurred only in 12 specimens; 9 of which had a dowel diameter of 6 mm, and the remaining 3 had a dowel diameter of 5 mm, with a pre-compression stress of 1 MPa. Based on the observations from the pre-experimental work, 4 mm was selected as the optimum dowel diameter for subsequent experiments. The individual results of the shear test for specimens with a 5 mm dowel diameter are given in Figure 10. a-b.

Preprints (www.preprints.org) | NOT PEER-REVIEWED | Posted: 17 April 2023 doi:10.20944/preprints202304.0444.v1

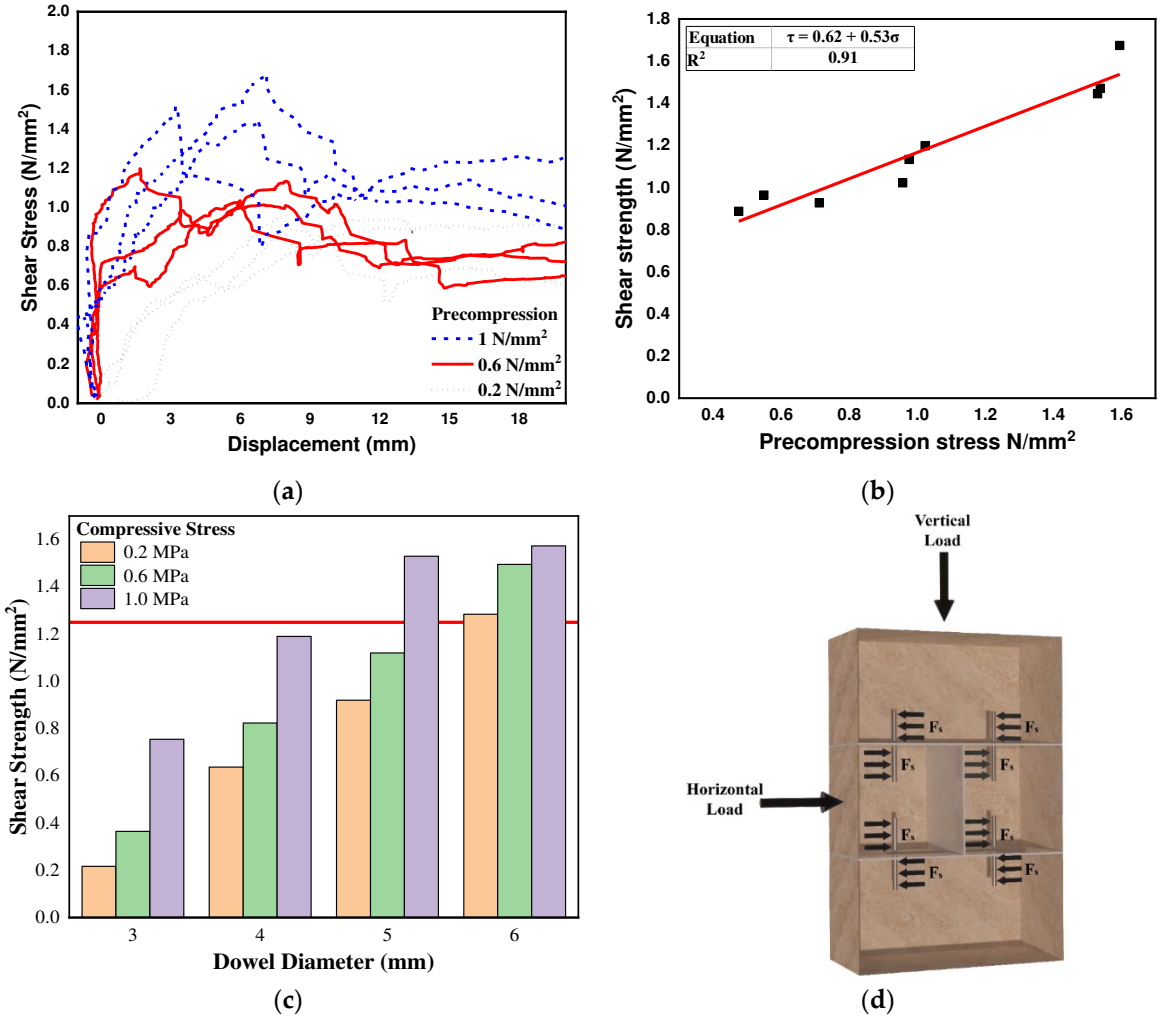

Figure 10. Triplet test results for determining the optimum dowel diameter: (**a**) Shear stress diagram for specimens with a 5 mm dowel diameter; (**b**) Shear strength vs precompression stress for specimens with a 5 mm dowel diameter; (**c**) Triplet test results of 36 dry joint specimens with different dowel diameter; (**d**) Exerted forces during the triplet test.

Moreover, the application of cramps was also investigated by simple compression tests. As shown in Figure 11. a and d, cramps can be applied in two ways. The first method is easy and simple, as it can be directly applied on the stone surface without carving a channel. The second method is relatively costly and difficult, in which a channel with a width and depth at least equal to the width and thickness of the cramp is carved. The second method is better, as there is only mortar in the joint. Thus, the compressive load exerted on the specimen is transferred uniformly by each stone element to the mortar and then to the stone beneath it. In the first method, as there are mortar and cramps in the joints, the abovementioned load is transferred by an individual stone onto the cramps and mortar and then to the stone beneath it. Due to the difference in the mechanical properties of cramps and mortar; the exerted load will be transferred only by cramps on the individual stone beneath it. Therefore, the load transferred by cramps is convened under a strip-like area, which acts as the tensile splitting force. As a result, the failure in individual stones is due to the tensile splitting force, not a compressive force, where the tensile splitting strength of the brittle materials (stone) is tremendously lower than their compressive strength. Therefore, a substantial drop in the compressive strength of the specimen may occur.

Preprints (www.preprints.org) | NOT PEER-REVIEWED | Posted: 17 April 2023 doi:10.20944/preprints202304.0444.v1

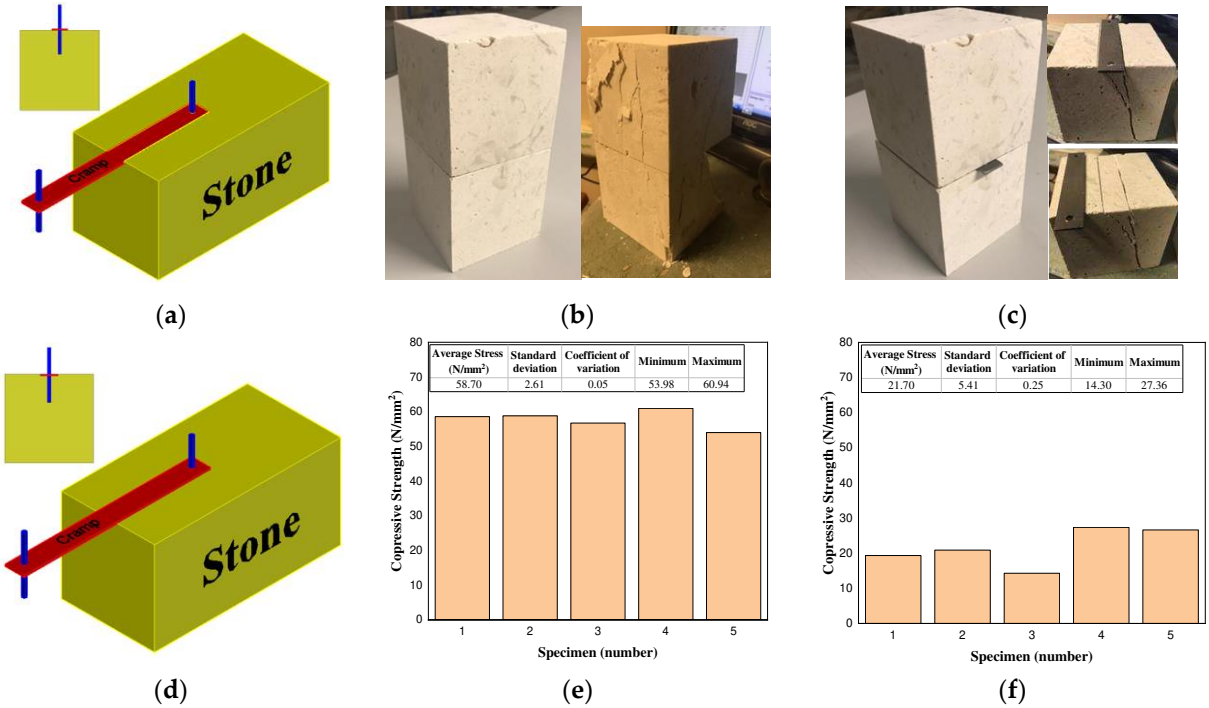

Figure 11. Compression test results for the application of cramps: (**a**) Application of cramps without carving individual stones; (**b**) Compression test specimen without cramps; (**c**) Compression test specimen with cramps; (**d**) Application of cramps with carving individual stones; (**e**) Compressive strength of specimens without the application of cramps; (**f**) Compressive strength of specimens with the application of cramps.

To quantify the drop in compressive strength of the wall under uniaxial force after applying the cramps directly on individual stone elements, a series of simple compression tests were carried out on 10 specimens with a size of 100 × 200 × 100 mm³ (width × height × length), which contained two 100 × 100 × 100 mm³ half stones placed on top of each other. Five of these specimens contained no cramps (Figure 11. b), whereas the remainder contained a cramp between the two half stones (Figure 11. c). The test results are shown in Figure 11. e and f.

3.2. Compressive strength

Table 4 summarizes the results of the compression tests carried out on both micro and macro-sized specimens, whose details are given in Section 2.3.2. The results of micro-sized specimens represent the average result of 3 specimens while the results of macro-sized specimens represent only one specimen's result. The failure of all compressive micro-sized specimens was sudden and highly brittle, while the macro-sized specimens exhibited more ductile fractures. However, it was observed that the failure of both specimens occurred at the maximum load. The visible cracks just started near the maximum load and caused specimen failure. The development of cracks was propagated parallel to uniaxial loading. Figure 12 shows the failure and the stress–strain diagram of specimens under compression.

Table 4. Compressive test results of micro and macro-sized specimens.

Specimen	Specimen size	f_i (N/mm²)	E (N/mm²)
SWC-01	Micro-sized	19.02	7369
SWLC-01		28.19	7490
SWMLC-01		23.47	5558
DWMLC-01		23.24	5394
MSWC	Macro-sized	7.20	4030

Preprints (www.preprints.org) | NOT PEER-REVIEWED | Posted: 17 April 2023 doi:10.20944/preprints202304.0444.v1

MSWLC	10.46	6177
MSWMLC	12.74	6416
MDWMLC	8.63	2716

f_i: Compressive strength.

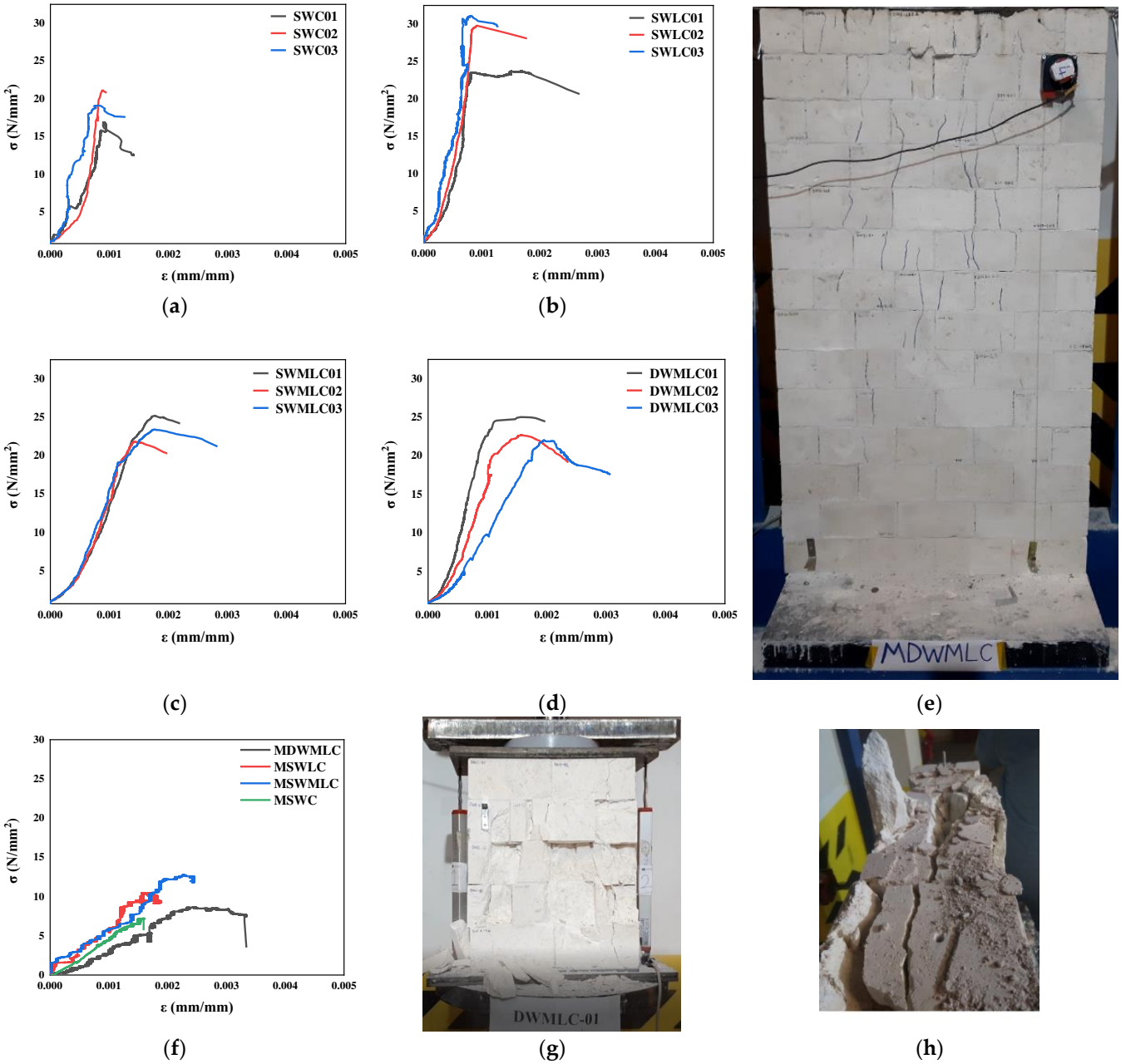

Figure 12. Failure and stress-strain diagrams of specimens under compression: (**a**) Stress–strain diagram of the SWC group; (**b**) Stress–strain diagram of the SWLC group; (**c**) Stress–strain diagram of the SWMLC group; (**d**) Stress–strain diagram of the DWMLC group; (**e**) Macro-sized specimen failure (MDWMLC); (**f**) Stress-strain diagram of macro-sized specimens; (**g**) Micro-sized specimen failure (DWMLC – outside of the wall); (**h**) Micro-sized specimen failure (DWMLC – inside of the wall).

3.3. Triplet test

In the triplet test, the failure of all specimens occurred by sliding the stone of the middle row, even for the specimens with metal connectors. As the optimum dowel diameter was used in the triplet tests, none of the individual stone units were split into two, but only the dowel cut-off was observed.

Preprints (www.preprints.org) | NOT PEER-REVIEWED | Posted: 17 April 2023 doi:10.20944/preprints202304.0444.v1

As expected, the shear strength of the specimens with metal connectors was higher than that of the specimens without metal connectors. It is important to remember that the level of pre-compressive stress plays a key role in the shear strength of individual specimens, and it is difficult to keep this stress constant, as proposed by the standard. Although a total of six rollers were placed beneath and above each specimen between two steel plates to allow horizontal movement, there was an increase in the pre-compressive stress. This increase was particularly higher in specimens with metal connectors. Therefore, this parameter was considered when calculating the shear strength (f_{voi}) values. The results of the shear test for all the specimens are given in Table 5, and the values of f_{vo} are given in Figure 13 for each type of wall.

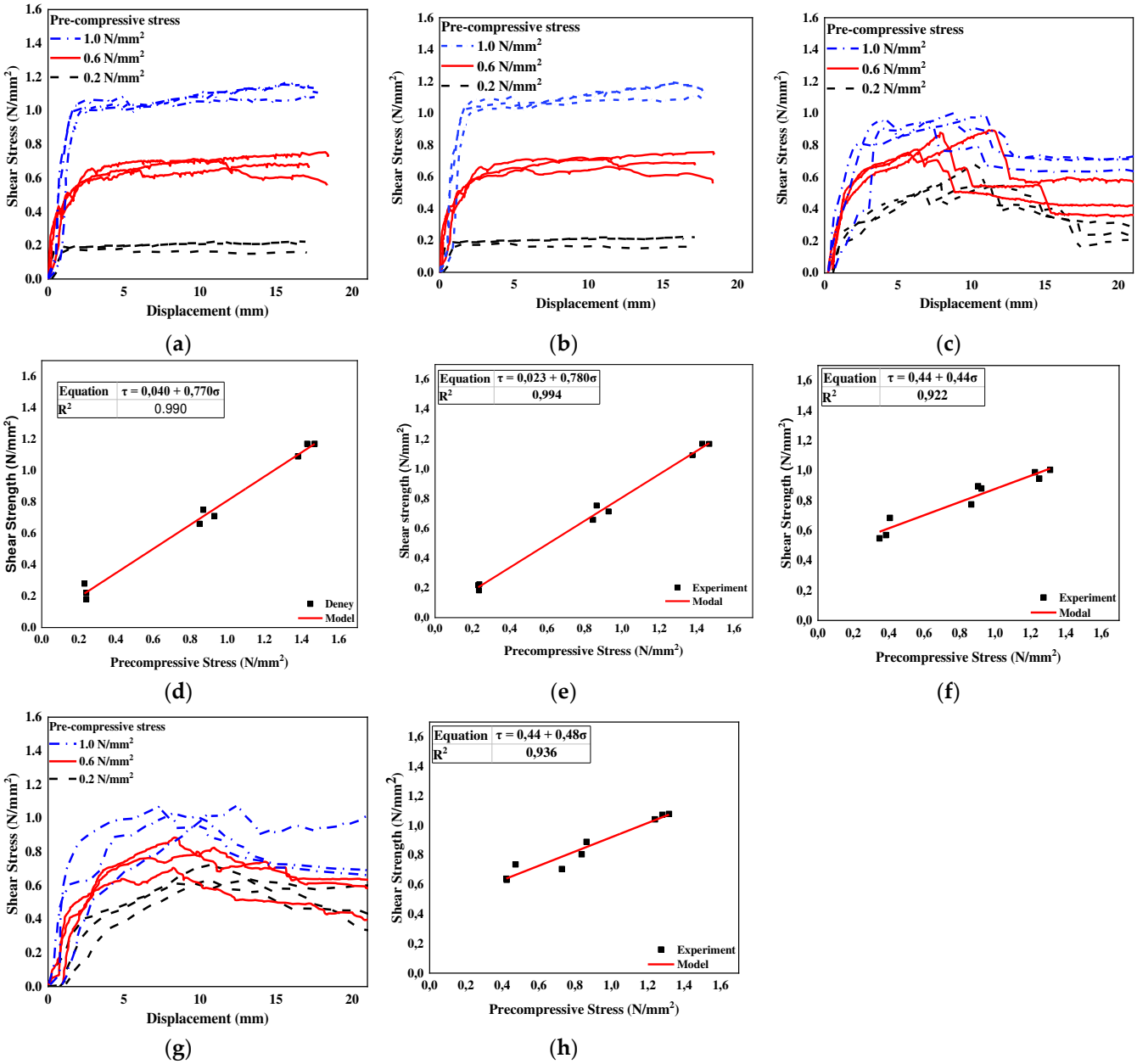

Figure 13. Triplet test results: (**a**) Shear stress-displacement diagram for the dry joint single layer specimen; (**b**) Shear stress-displacement for the single layer specimen without metal connectors; (**c**) Shear stress-displacement for the single layer specimen with metal connectors; (**d**) Shear strength versus normal stress plots for dry joint single walls; (**e**) Shear strength versus normal stress plots for single walls without metal connectors; (**f**) Shear strength versus normal stress plots for single walls with metal connectors; (**g**) Shear stress-displacement for the double layer specimen without metal connectors; (**h**) Shear strength versus normal stress plots for double walls without metal connectors.

Preprints (www.preprints.org) | NOT PEER-REVIEWED | Posted: 17 April 2023 doi:10.20944/preprints202304.0444.v1

Table 5. Triplet test results of 36 micro-sized specimens.

Specimen Code	Stan. Comp.[1] Stress (N/mm²)	Avg. Appl.[2] Comp. Stress (N/mm²)	Avg. Shear Force (N)	Avg. Shear Stress (N/mm²)
SWIS20	0.2	0.24	7840	0.23
SWIS60	0.6	0.88	26881	0.71
SWIS100	1.0	1.43	43091	1.17
SWMLIS20	0.2	0.38	22829	0.6
SWMLIS60	0.6	0.90	32523	0.85
SWMLIS100	1.0	1.26	37438	0.98
DWMLIS20	0.2	0.44	50399	0.67
DWMLIS60	0.6	0.81	61076	0.80
DWMLIS100	1.0	1.28	81052	1.06

[1]Standart compressive stress. [2]Average applied compressive stress.

3.4. Diagonal compression test

According to ASTM E 519M-15 standard, the shear strength of masonry walls was calculated using Equation 4, where P stands for applied force and A_n for the area. This equation evaluates the shear strength in the middle of the wall. This means that the Mohr circle is centered in the τ-σ plane [63]. In addition, Shear Strain (γ) and Modulus of Rigidity (G) was calculated with Equation 5 and 6. In Equation 5, ε_t represents tension and ε_c represents compression strains which were calculated as the average of the readings from LVDTs mounted on both sides of the wall specimens.

$$\tau = 0.707 \times P/A_n, \quad (4)$$

$$\gamma = \varepsilon_t + \varepsilon_c \quad (5)$$

$$G = \tau/\gamma \quad (6)$$

Currently, regulations and modern design approaches do not only consider strength in structural analysis. In addition, it attaches great importance to the displacements that occur in the building. Although it is known that conventional masonry buildings exhibit brittle behavior against earthquakes, according to regulations, these buildings can deform significantly before collapsing. This can be explained by the assumption that deformation occurs beyond the elastic limit with cracks in the building. Thus, the energy generated is distributed by the structure without loss of strength against vertical loads. This approach imparts significant pseudo-ductile behavior beyond the elastic region to masonry walls composed of brittle individual elements such as stone, brick, and mortar [53,64]. The ductility of the DCT specimens was calculated with Equation 7.

$$\mu = \gamma_u/\gamma_y \quad (7)$$

In Equation 7, μ represents the DCT specimen's ductility, γ_u is the ultimate shear strain and γ_y is the yield strain. The ultimate strain is calculated as the post-peak strain corresponding to the stress with a reduction of 20% in peak stress. As for yield strain, it was calculated from bilinear curves which is the idealized form of force-strain curves obtained from the experimental campaign.

Table 6. Diagonal compression test results.

Specimens	F_{max} (N)	Avg. F_{max} (N)	τ (N/mm²)	Avg. τ (N/mm²)	γ_u	γ_y	μ	Avg. μ	Avg. G
SWLDT-01	47953		0.28		0.00190	0.00190	1		
SWLDT-02	46449	48955	0.27	2.29	0.00188	0.00188	1	1	118
SWLDT-03	52463		0.31		0.00090	0.00090	1		
SWMDT-01	46165	45975	0.27	0.27	0.00100	0.01060	11	13	366
SWMDT-02	41898		0.24		0.00041	0.00811	20		

Preprints (www.preprints.org) | NOT PEER-REVIEWED | Posted: 17 April 2023 doi:10.20944/preprints202304.0444.v1

SWMDT-03	49863		0.29		0.00078	0.00571	7		
DWMDT-01	91760		0.27		0.00139	0.04715	34		
DWMDT-02	89850	92709	0.26	0.27	0.00108	0.04615	43	33	186
DWMDT-03	96515		0.28		0.00148	0.03180	22		

Three different wall types were tested in the diagonal compression test. The first of these wall specimens were built as a single layer and only 2 mm of thickness lime mortar was used in the joints. The second wall type was also built as a single layer and the difference was the use of lime mortar + metal connectors in the joints. The third wall specimens were built of two layers with lime mortar + metal connectors and represent the proposed multi-leaf wall. It has been observed that each wall type has its unique failure pattern. While the first wall specimens exhibited a very brittle behavior where the cracks started just near the maximum load. On the other hand, with the initiation of cracks in the second wall type, a part of the wall was separated, and the compression load started to drop (Figure 14). The third wall specimen showed a more ductile failure. During the experiment, cracks formed at the joints parallel to the load, but the dowels came out of their holes as the cracks widened, which caused a drop in compression load and increments in displacement. The stress-strain diagram, bilinear curve, and failure pattern of all three wall specimen types are given in Figure 15.

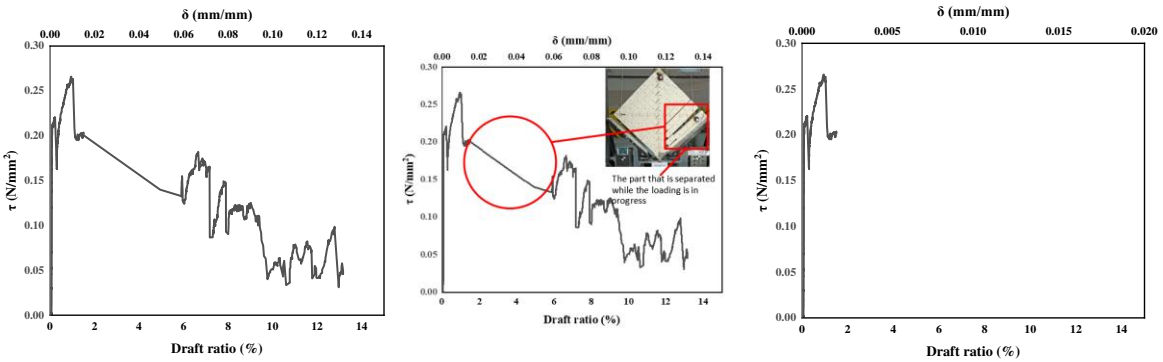

(**a**) (**b**) (**c**)

Figure 14. Modification process for specimens built with lime mortar + metal connectors: (**a**) Schematic stress-strain diagram of the SWMDT group; (**b**) Separation of part of the wall and its effect on the stress-strain diagram; (**c**) Modified stress-strain diagram for SWMDT group.

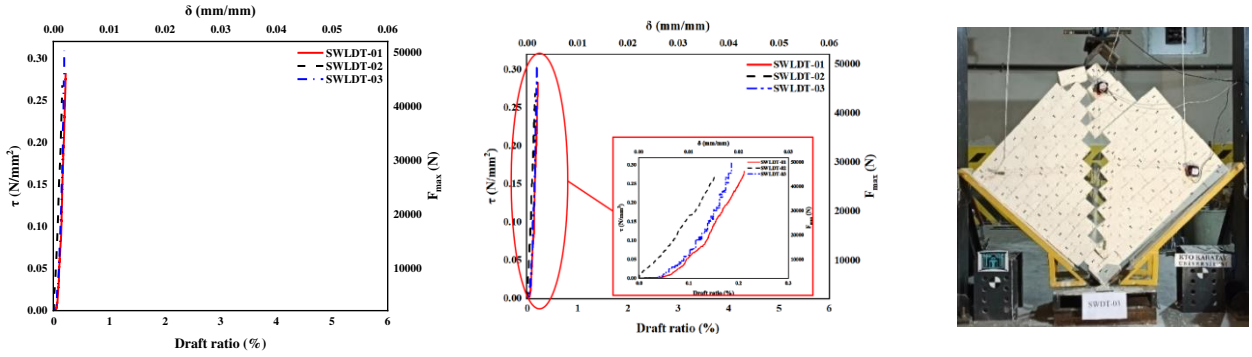

(**a**) (**b**) (**c**)

Preprints (www.preprints.org) | NOT PEER-REVIEWED | Posted: 17 April 2023 doi:10.20944/preprints202304.0444.v1

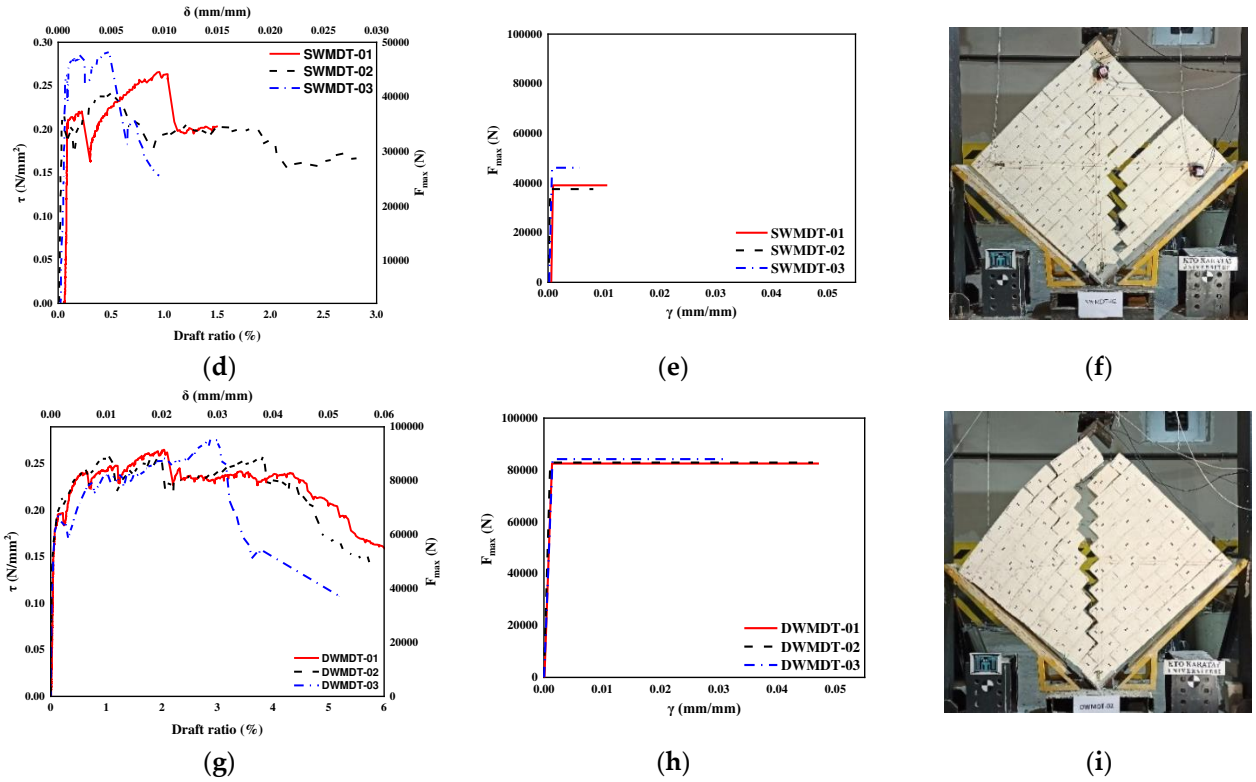

Figure 15. Diagonal compression test results: (**a**) Stress-strain diagram of the SWLDT group; (**b**) Stress-strain diagram of the SWLDT group; (**c**) Failure patterns for SWLDT group; (**d**) Modified stress-strain diagram of the SWMDT group; (**e**) Bilinear graph of the SWMDT group; (**f**) Failure patterns for SWMDT group; (**g**) Modified stress-strain diagram of the DWMDT group; (**h**) Bilinear graph of the DWMDT group; (**i**) Failure patterns for DWMDT group.

4. Discussion

4.1. Compression

To determine the compressive strength of the proposed multi-leaf wall, two different specimen sizes were used. The reason for this is to investigate the slenderness ratio (h_{ef}/t_{ef}) which is the ratio of effective height to effective width. Considering the results, a decrease of around 90% is observed in the compressive strength of the wall due to the size effect.

The comparison of compressive test results for both micro- and macro-sized wall specimens is depicted in Figure 16. The failure mode for both specimen sizes was approximately the same. It was observed that the failure occurred close to the maximum axial load. However, the failure of the micro-sized samples was sudden and explosive, while the failure of the macro-sized specimens exhibited a more ductile feature. It has been observed that cracks in the macro-sized wall specimens occur close to the maximum load and propagated parallel to the load, causing the specimen's failure.

Preprints (www.preprints.org) | NOT PEER-REVIEWED | Posted: 17 April 2023 doi:10.20944/preprints202304.0444.v1

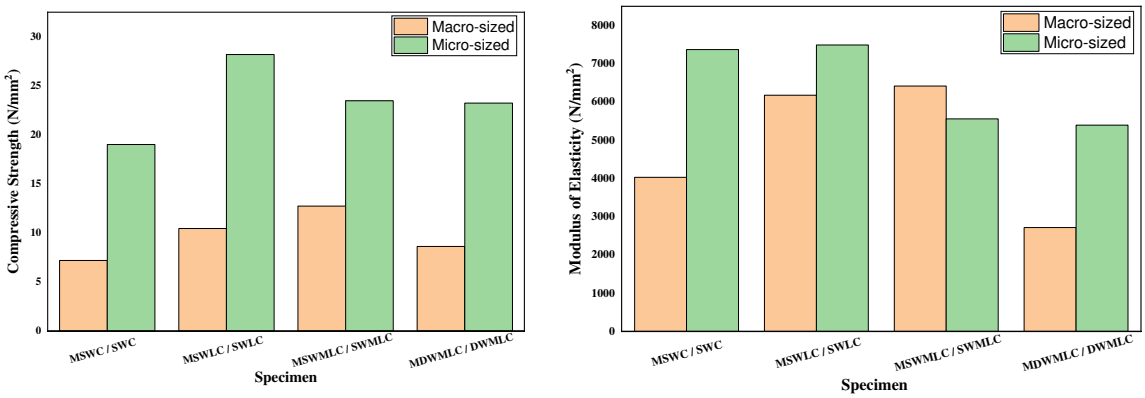

(**a**) (**b**)

Figure 16. Compression test result for micro and macro-sized specimens: (**a**) Comparison of compressive strength of micro and macro-sized walls; (**b**) Comparison of modulus of elasticity of micro and macro-sized walls.

When the results are compared, the difference in the compressive strength of the dry joint and the specimen with 2 mm lime mortar is approximately 39% and 37% respectively for micro and macro-sized specimens. Although the mechanical properties of lime mortar were weaker than those of stone, the specimen with 2 mm lime mortar had a higher compressive strength. This can be explained by the stone used in the experiments being highly brittle and the individual stones not being perfectly sawed; hence, the uniaxial forces were not transferred uniformly, leading to a 9 and 3 MPa drop in the strength of micro and macro-sized specimens respectively. However, for the specimens with 2 mm of mortar, the imperfections in the individual stone dimensions were quenched by the mortar, and the load transfer was more uniform.

For the single-leaf specimens with 2 mm mortar and specimens with mortar + metal connectors, there is a difference of approximately 18% in the compressive strength of micro-sized specimens, whereas the specimen with 2 mm mortar exhibited a higher strength. A drop in the compressive strength was expected due to the direct application of cramps over the individual stone units without carving a proper channel for them, but the drop was less than expected. As in Section 3.1, the drop in the compressive strength of the stone prisms was quantified by a simple compression test, and the results are provided in Figure 11. When the results were examined, the drop in the compressive strength of the stone prisms due to the direct application of cramps was approximately 92%, which is five times more than the drop observed from the compression test carried out on micro-sized specimens. However, the results of the macro-sized specimens show the opposite. The direct application of the cramps caused the compressive strength not to decrease but to increase on the contrary. This increase was around 19%.

For the multi-leaf stone wall, decreases of 30%, 53%, and 78% in the compressive strength were reported by Binda et al. [65], Demir, C. & İlki, A. [10] and Silva et al. [66], respectively, in contrast to the single leaf wall. However, in this study, a drop in the compressive strength of 1% in micro-sized and 38% in macro-sized specimens was observed between the single- (lime + metal connectors) and multi-leaf walls.

The ratio of Young's modulus is assumed to be the slope of the compressive strength curve, which is usually assumed to be between 20% and 50% of the mentioned slope [10]. However, in this study, as reported in [67], Young's modulus was evaluated according to EN 1052-1, which is calculated as the ratio of the compressive stress to strain that corresponds to one-third of the maximum stress. A summary of Young's modulus results for micro- and macro-sized specimens is depicted in Figure 16. b.

4.2. Shear

Preprints (www.preprints.org) | NOT PEER-REVIEWED | Posted: 17 April 2023 doi:10.20944/preprints202304.0444.v1

4.2.1. Triplet test

After evaluating the results of the triplet test on 36 specimens, the shear strength of the specimens substantially increased with an increase in the pre-compressive stress for dry joint specimens and the specimen with 2 mm lime mortar (SWIS and SWLIS), as expected. However, the results were different for specimens with metal connectors, as shown in Figure 13. c and g. The effect of metal connectors was approximately three times higher at a lower pre-compressive stress, but almost no effect was observed at a higher pre-compressive stress. Although it appears to be a trivial issue for evaluating the effect of metal connectors on the behavior of the shear strength of a specimen, it is significant when the results of 9 specimens are evaluated by applying linear regression to quantify the parameters of the shear strength for the different wall types, which are the initial shear strength (f_{vo}). The relationship between the pre-compressive and shear stresses is shown in Figure 13. d-f and h. Note that keeping the level of pre-compressive stress constant is nearly impossible, particularly for specimens with metal connectors. Therefore, while applying linear regression, the level of pre-compressive stress that corresponds to the maximum shear strength was considered. Figure 17 shows the values of f_{vo} and α (friction angle) for different types of wall specimens exposed to the shear test. As seen in Figure 17, the effect of metal connectors on the initial shear parameters of the proposed wall was significant.

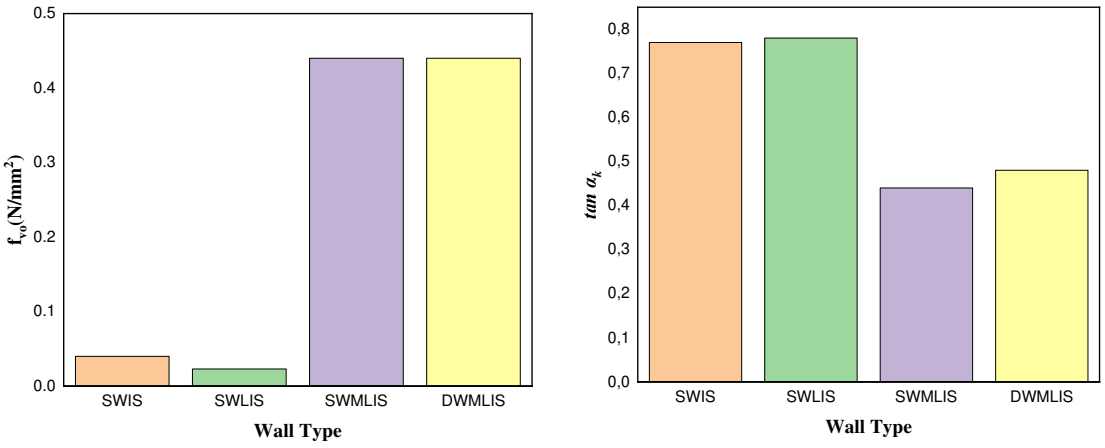

Figure 17. Initial shear strength f_{vo} and angle of friction (α) values for different wall types. (**a**) Initial shear strength f_{vo}; (**b**) Angle of friction (α).

Figure 17 demonstrates that the initial shear strength depends first on the level of compressive stress and then on the mechanical properties of the joint, which are surface friction for a dry joint, cohesive behavior for a mortar joint, and shear strength of dowels for joints with metal connectors. As shown in Figure 17. a, the initial shear of the SWIS (dry joint) walls is higher than that of the SWLIS (mortar joint) walls. This can be explained by the fact that the thickness of the joints in the SWLIS walls is 2 mm. Due to the thin layer of mortar and poor mechanical properties, the mortar joint has a negligible effect on the shear strength of the joint. In addition, it could be argued that the aggregate with a 2 mm diameter used in the mortar acts like small roller balls, which reduces the surface friction. This results in a reduction in the shear strength. However, for dry joints, the rough surface helps increase the surface friction as well as the shear strength. In contrast, the massive increase in the shear strength of the specimen containing joints with metal connectors is intuitive due to the four dowels, which take on the shear force applied to the joints. The increase in the shear strength with the use of metal connectors was approximately 11 times greater than that of the dry joint and 19 times greater than that of the mortar joint. The difference in the maximum shear force corresponding to the shear strength of the multi-leaf wall compared to a single-layer wall is twice that expected due to the shear area and the number of dowels used in the specimen.

Preprints (www.preprints.org) | NOT PEER-REVIEWED | Posted: 17 April 2023 doi:10.20944/preprints202304.0444.v1

Another important topic to be discussed is the energy absorption of the specimens. This topic is controversial in masonry buildings, particularly in stone masonry walls, due to the brittle materials (stone + mortar) used in the wall. However, we evaluated the energy absorption capacities for various wall types from the triplet test, due to the metal connectors used in the proposed wall. The energy absorption capacities of the walls can be calculated from the shear force–displacement curve, where the area under the curve indicates the energy absorption capacity. In Figure 18, the representative shear force–displacement curve for walls with metal connectors and walls without metal connectors are given. As shown in Figures 18. a and c, the failure of the specimens under shear forces is different for each wall type, where Figure 18. a represents the wall type with dry or mortar joints, and Figure 18. c represents joints with metal connectors. Both failure types show a characteristic behavior, despite their differences. After attaining the maximum shear force and failure of the joint, the shear force takes an approximately constant value under pre-compressive stress, where the displacement increases. Considering the entire area under this curve will not be realistic. Therefore, shear force–displacement curve were modified, as shown in Figure 18. b and d. In the modification process, the displacement corresponding to the maximum shear force was considered. Then, the energy absorption for each wall type was calculated as the area under the force–displacement curve, where the maximum shear force occurs. Figure 18. e shows the energy absorption capacities for various wall types.

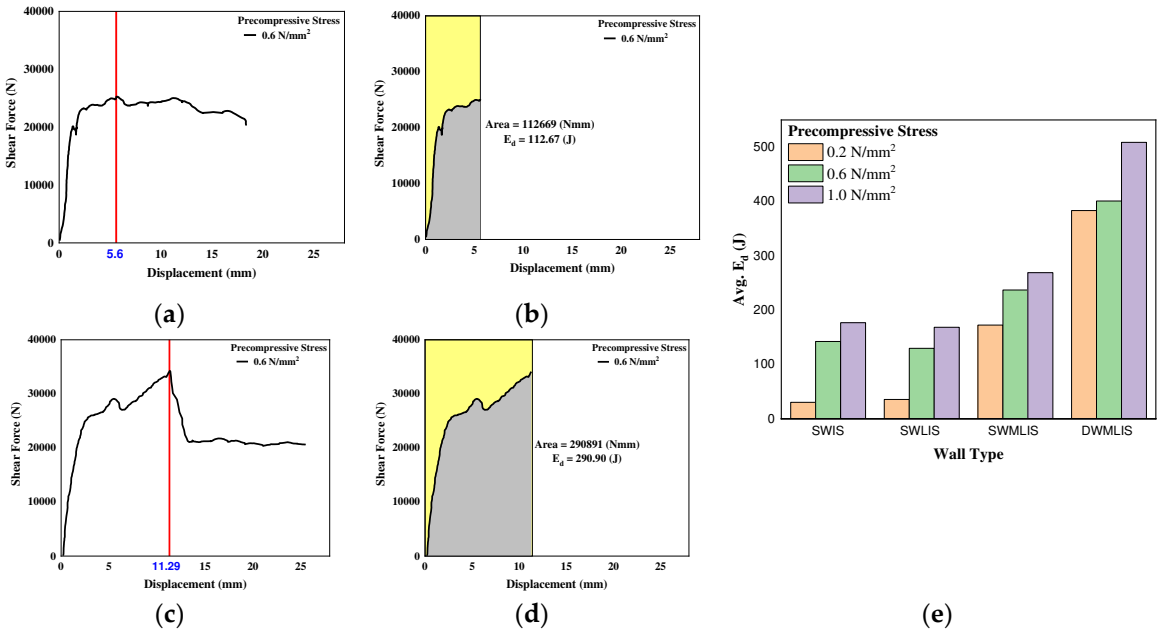

Figure 18. Obtained and modified shear force–displacement diagrams for energy absorption calculations. (**a**) Shear force–displacement diagram of walls with dry and mortar joints; (**b**) Modified shear force–displacement diagram of walls with dry and mortar joints; (**c**) Shear force–displacement diagram of walls with joints reinforced with metal connectors; (**d**) Modified shear force–displacement diagram of walls with joints reinforced with metal connectors; (**b**) Energy absorption capacity for different wall types.

4.2.2. Diagonal compression test

Table 6 shows the shear strengths of three wall types subjected to diagonal compression tests. According to the results, shear strength for all wall types is approximately identical. The effect of metal connectors on the shear strength of wall specimens is not fully understood in the diagonal compression test since vertical loads are very low. This effect is particularly evident in single-leaf specimens that have lime mortar and metal connectors in their joints. The failure in these specimens was caused by a portion of the wall being separated from the wall in a direction that was approximately perpendicular to the shear plane. Consequently, it's been observed that no cut-off

Preprints (www.preprints.org) | NOT PEER-REVIEWED | Posted: 17 April 2023 doi:10.20944/preprints202304.0444.v1

occurred in the metal connectors, especially in the dowels. It was due to the diameter of the dowel's holes being 1 mm larger than the dowel diameter and no filling material being used in the holes, so the dowel just slipped out of the hole and the specimen failed. Although the shear strength of the three wall types is approximately the same, the contribution of the metal connectors is quite significant in terms of ductility (Figure 19. a) and energy absorption (Figure 19. b). The ductility criterion was calculated by taking 3 specimen test results. Figure 19. a shows the ductility of a single-leaf specimen (SWMDT) with metal connectors as it is approximately five times higher than the average ductility level of lime mortar specimens (SWLDT). Additionally, when comparing single (SWMDT) and multi-leaf (DWMDT) specimens containing metal connectors, it was determined that multi-leaf specimen ductility was 2.5 times higher than single-leaf. The energy absorption capacity of wall specimens is determined by the ductility levels, so the same can be applied to the energy absorption.

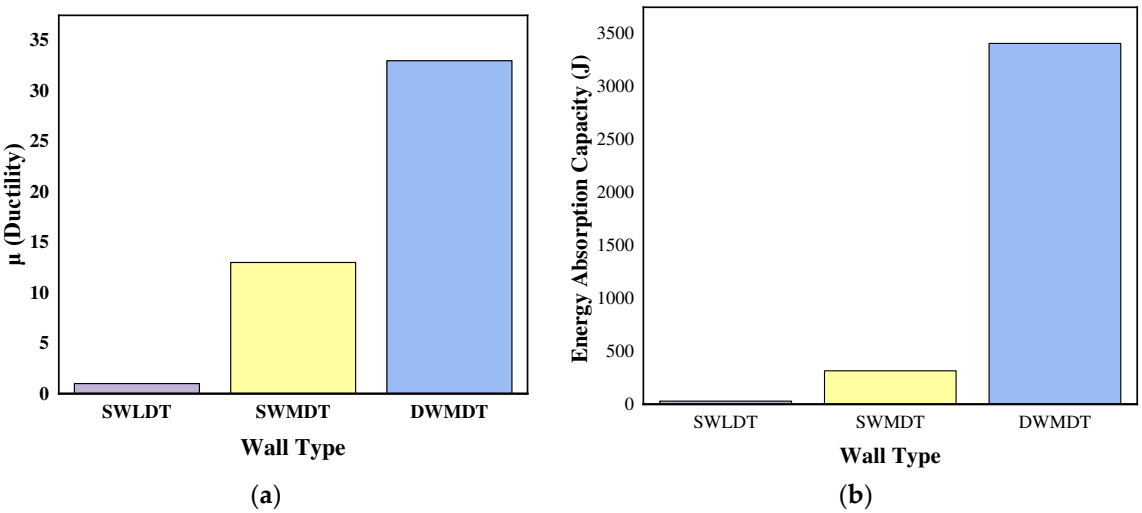

Figure 19. Ductility and energy absorption values calculated from the diagonal compression test. (**a**) Ductility values for three wall types; (**b**) Energy absorption capacity for three wall types.

5. Conclusions

In this study, a stone multi-leaf wall with a new load-bearing mechanism was designed and proposed for modern natural stone masonry buildings that meet the current building requirements. The primary purpose of this study was to experimentally investigate the in-plane behaviors of the proposed wall. In addition, this study aimed to pave the way for the construction of natural stone masonry buildings, which are both modern and have a monumental identity with ecological architecture and a service life of more than building built with currently used construction materials (reinforced concrete buildings).

The proposed multi-leaf stone masonry wall consists of two layers and a cavity between them. To secure the integrity of the wall, the layers are connected with metal connectors designed in this study. The design aims to reduce the total weight of the building by omitting the middle layer and concealing all installations needed in the building.

The primary experimental investigation of the shear and compressive strength behaviors showed that the advantages of the metal connectors in improving the strength capacity of the wall outweigh their disadvantages.

In summary, the application of dowels substantially increased the shear capacity of the wall, whereas the direct application of cramps on individual stone units, which substantially reduced the application cost, did not lead to a drop in the compressive strength, as expected. This is a positive sign and guidance for the further investigation of mechanical behavior.

Author Contributions: Conceptualization, A.J.Z.; methodology, A.J.Z.; resources, A.İ.; writing—original draft preparation, A.J.Z.; writing—review and editing, A.J.Z., A.İ.; supervision, A.İ.; funding acquisition, A.İ. All authors have read and agreed to the published version of the manuscript.

Funding: This research received no external funding.

Acknowledgments: This study is a port of Ph.D. thesis of Dr. Ahmad Javid ZIA entitled "Experimental Investigation of Multi-Layered Cut Stone Walls" and the authors would like to thank staff of the Structural Mechanics Laboratory, Department of Civil Engineering, KTO Karatay University for help and support.

Conflicts of Interest: The authors declare no conflict of interest.

References

1. Hendry, A.W.; Khalaf, F.M. Masonry Wall Construction; 2001; Vol. 39; ISBN 0415232821.
2. Wright, G.R.. Ancient Building Technology; 3rd ed.; Brill: 3. Cilt, Leiden, Boston, 2009; ISBN 9783540773405.
3. Jing, J.; Zhou, C.; Zhang, C.; Li, T. In-Plane Cyclic Behavior of Brick Walls Strengthened with CFRP Plates Embedded in the Horizontal Mortar Joint. J. Build. Eng. 2023, 63, 105476, doi:10.1016/j.jobe.2022.105476.
4. Gkournelos, P.D.; Triantafillou, T.C.; Bournas, D.A. Seismic Upgrading of Existing Masonry Structures: A State-of-the-Art Review. Soil Dyn. Earthq. Eng. 2022, 161, 107428, doi:10.1016/j.soildyn.2022.107428.
5. Abdulsalam, B.; Ali, A.H.; ElSafty, A.; Elshafey, N. Behavior of GFRP Strengthening Masonry Walls Using Glass Fiber Composite Anchors. Structures 2021, 29, 1352–1361, doi:10.1016/j.istruc.2020.12.025.
6. Anglade, E.; Giatreli, A.; Blyth, A.; Di, B.; Parisse, F.; Namourah, Z.; Rodrigues, H.; Miguel, T. International Journal of Disaster Risk Reduction Seismic Damage Scenarios for the Historic City Center of Leiria , Portugal : Analysis of the Impact of Different Seismic Retrofitting Strategies on Emergency Planning. Int. J. Disaster Risk Reduct. 2020, 44, 101432, doi:10.1016/j.ijdrr.2019.101432.
7. Rotunno, T.; Fagone, M.; Bertolesi, E.; Grande, E.; Milani, G. Curved Masonry Pillars Reinforced with Anchored CFRP Sheets : An Experimental Analysis. Compos. Part B 2019, 174, 107008, doi:10.1016/j.compositesb.2019.107008.
8. Kumar, P.; Rao, V.; Singh, Y. Out-of-Plane Flexural Behaviour of Masonry Wallettes Strengthened Using FRP Composites and Externally Bonded Grids : Comparative Study. Compos. Part B 2019, 176, 107302, doi:10.1016/j.compositesb.2019.107302.
9. Orlando, M.; Betti, M.; Spinelli, P. Assessment of Structural Behaviour and Seismic Retrofitting for an Italian Monumental Masonry Building. J. Build. Eng. 2020, 29, 101115, doi:10.1016/j.jobe.2019.101115.
10. Demir, C.; Ilki, A. Characterization of the Materials Used in the Multi-Leaf Masonry Walls of Monumental Structures in Istanbul, Turkey. Constr. Build. Mater. 2014, 64, 398–413, doi:10.1016/j.conbuildmat.2014.04.099.
11. García, D.; San-José, J.T.; Garmendia, L.; Larrinaga, P. Comparison between Experimental Values and Standards on Natural Stone Masonry Mechanical Properties. Constr. Build. Mater. 2012, 28, 444–449.
12. Oliveira, D. V.; Lourenço, P.B.; Roca, P. Cyclic Behaviour of Stone and Brick Masonry under Uniaxial Compressive Loading. Mater. Struct. 2006, 39, 247–257.
13. Buzov, A.; Radnić, J.; Grgić, N. Effects of Several Bolt Parameters on the Bearing Capacity of a Composite Multi-Drum Stone Column under an Earthquake. Compos. Part B Eng. 2019, 162, 250–258, doi:10.1016/j.compositesb.2018.10.104.
14. Muñoz, R.; Lourenço, P.B.; Moreira, S. Experimental Results on Mechanical Behaviour of Metal Anchors in Historic Stone Masonry. Constr. Build. Mater. 2018, 163, 643–655, doi:10.1016/j.conbuildmat.2017.12.090.
15. Vintzileou, E.; Miltiadou-Fezans, A. Mechanical Properties of Three-Leaf Stone Masonry Grouted with Ternary or Hydraulic Lime-Based Grouts. Eng. Struct. 2008, 30, 2265–2276.
16. Almeida, C.; Guedes, J.P.; Arêde, A.; Costa, C.Q.; Costa, A. Physical Characterization and Compression Tests of One Leaf Stone Masonry Walls. Constr. Build. Mater. 2012, 30, 188–197.
17. Silva, B.; Dalla Benetta, M.; Da Porto, F.; Modena, C. Experimental Assessment of In-Plane Behaviour of Three-Leaf Stone Masonry Walls. Constr. Build. Mater. 2014, 53, 149–161, doi:10.1016/j.conbuildmat.2013.11.084.
18. Gattesco, N.; Boem, I. Out-of-Plane Behavior of Reinforced Masonry Walls: Experimental and Numerical Study. Compos. Part B Eng. 2017, 128, 39–52, doi:10.1016/j.compositesb.2017.07.006.
19. Meimaroglou, N.; Mouzakis, H. Mechanical Properties of Three-Leaf Masonry Walls Constructed with Natural Stones and Mud Mortar. Eng. Struct. 2018, 172, 869–876, doi:10.1016/j.engstruct.2018.06.015.

20. Maccarini, H.; Vasconcelos, G.; Rodrigues, H.; Ortega, J.; Lourenço, P.B. Out-of-Plane Behavior of Stone Masonry Walls: Experimental and Numerical Analysis. Constr. Build. Mater. 2018, 179, 430–452, doi:10.1016/j.conbuildmat.2018.05.216.
21. Pulatsu, B.; Erdogmus, E.; Lourenço, P.B.; Lemos, J. V.; Tuncay, K. Simulation of the In-Plane Structural Behavior of Unreinforced Masonry Walls and Buildings Using DEM. Structures 2020, 27, 2274–2287, doi:10.1016/j.istruc.2020.08.026.
22. Drougkas, A.; Roca, P.; Molins, C. Numerical Prediction of the Behavior, Strength and Elasticity of Masonry in Compression. Eng. Struct. 2015, 90, 15–28, doi:10.1016/j.engstruct.2015.02.011.
23. Andreotti, G.; Graziotti, F.; Magenes, G. Detailed Micro-Modelling of the Direct Shear Tests of Brick Masonry Specimens: The Role of Dilatancy. Eng. Struct. 2018, 168, 929–949, doi:10.1016/j.engstruct.2018.05.019.
24. Francisco, S.; Council, A.T. Improving the Seismic Performance of Existing Buildings and Other Structures. 2009, 75–84.
25. Juhásová, E.; Sofronie, R.; Bairrão, R. Stone Masonry in Historical Buildings - Ways to Increase Their Resistance and Durability. Eng. Struct. 2008, 30, 2194–2205, doi:10.1016/j.engstruct.2007.07.008.
26. Silva, M.B. Percepção Da População Assistida Sobre a Inserção de Estudantes de Medicina Na Unidade Básica de Saúde. Trab. conclusão curso 2016, 1, 1–10, doi:10.1017/CBO9781107415324.004.
27. Acito, M.; Magrinelli, E.; Milani, G.; Tiberti, S. Seismic Vulnerability of Masonry Buildings: Numerical Insight on Damage Causes for Residential Buildings by the 2016 Central Italy Seismic Sequence and Evaluation of Strengthening Techniques. J. Build. Eng. 2020, 28, 101081, doi:10.1016/j.jobe.2019.101081.
28. EN 1052-3 Methods of Test for Masonry — Part 3: Determination of Initial Shear Strength; European Committee for Standardization, 2002;
29. ASTM E 519M-15 Standard Test Method for Diagonal Tension (Shear) in Masonry Assemblages 2015.
30. EN 1052-1 Methods of Test for Masonry - Part 1: Determination of Compressive Strength; European Committee for Standardization, 1999;
31. Boscato, G.; Reccia, E.; Cecchi, A. Non-Destructive Experimentation: Dynamic Identification of Multi-Leaf Masonry Walls Damaged and Consolidated. Compos. Part B Eng. 2018, 133, 145–165, doi:10.1016/j.compositesb.2017.08.022.
32. Borri, A.; Corradi, M.; Castori, G.; Molinari, A. Stainless Steel Strip – A Proposed Shear Reinforcement for Masonry Wall Panels. Constr. Build. Mater. 2019, 211, 594–604, doi:10.1016/j.conbuildmat.2019.03.197.
33. Silva, B.; Dalla Benetta, M.; Da Porto, F.; Modena, C. Experimental Assessment of In-Plane Behaviour of Three-Leaf Stone Masonry Walls. Constr. Build. Mater. 2014, 53, 149–161, doi:10.1016/j.conbuildmat.2013.11.084.
34. Cotič, P.; Jagličić, Z.; Bosiljkov, V. Validation of Non-Destructive Characterization of the Structure and Seismic Damage Propagation of Plaster and Texture in Multi-Leaf Stone Masonry Walls of Cultural-Artistic Value. J. Cult. Herit. 2014, 15, 490–498, doi:10.1016/j.culher.2013.11.004.
35. Cascardi, A.; Leone, M.; Aiello, M.A. Transversal Joining of Multi-Leaf Masonry through Different Types of Connector: Experimental and Theoretical Investigation. Constr. Build. Mater. 2020, 265, 120733, doi:10.1016/j.conbuildmat.2020.120733.
36. Rezaie, A.; Godio, M.; Beyer, K. Experimental Investigation of Strength, Stiffness and Drift Capacity of Rubble Stone Masonry Walls. Constr. Build. Mater. 2020, 251, 118972, doi:10.1016/j.conbuildmat.2020.118972.
37. Tiberti, S.; Milani, G. 3D Homogenized Limit Analysis of Non-Periodic Multi-Leaf Masonry Walls. Comput. Struct. 2020, 234, 106253, doi:10.1016/j.compstruc.2020.106253.
38. Graziotti, F.; Tomassetti, U.; Penna, A.; Magenes, G. Out-of-Plane Shaking Table Tests on URM Single Leaf and Cavity Walls. Eng. Struct. 2016, 125, 455–470, doi:10.1016/j.engstruct.2016.07.011.
39. Tomassetti, U.; Graziotti, F.; Penna, A.; Magenes, G. Modelling One-Way out-of-Plane Response of Single-Leaf and Cavity Walls. Eng. Struct. 2018, 167, 241–255, doi:10.1016/j.engstruct.2018.04.007.
40. Arslan, O.; Messali, F.; Smyrou, E.; Bal, İ.E.; Rots, J.G. Experimental Characterization of the Axial Behavior of Traditional Masonry Wall Metal Tie Connections in Cavity Walls. Constr. Build. Mater. 2020, 266, doi:10.1016/j.conbuildmat.2020.121141.
41. Giaretton, M.; Dizhur, D.; da Porto, F.; Ingham, J.M. Construction Details and Observed Earthquake Performance of Unreinforced Clay Brick Masonry Cavity-Walls. Structures 2016, 6, 159–169, doi:10.1016/j.istruc.2016.04.004.

42. Derakhshan, H.; Lucas, W.; Visintin, P.; Griffith, M.C. Out-of-Plane Strength of Existing Two-Way Spanning Solid and Cavity Unreinforced Masonry Walls. Structures 2018, 13, 88–101, doi:10.1016/j.istruc.2017.11.002.
43. Xiao, J.; Pu, J.; Hu, Y. Experimental Study on the Compressive Performance of New Sandwich Masonry Walls. Front. Struct. Civ. Eng. 2013, 7, 154–163, doi:10.1007/s11709-013-0203-0.
44. Corradi, M.; Borri, A.; Poverello, E.; Castori, G. The Use of Transverse Connectors as Reinforcement of Multi-Leaf Walls. Mater. Struct. 2017, 50, 114.
45. EN 1926 Natural Stone Test Methods — Determination of Uniaxial Compressive Strength; European Committee for Standardization, 2006;
46. EN 12372 Natural Stone Test Methods — Determination of Flexural Strength under Concentrated Load; European Committee for Standardization, 2006;
47. EN 14580 Natural Stone Test Methods — Determination of Static Elastic Modulus; European Committee for Standardization, 2006; Vol. 3, p. 15;.
48. Isabel, A.; Morais, J.; Morais, P.; Veiga, R.; Santos, C.; Candeias, P.; Gomes, J. Modulus of Elasticity of Mortars : Static and Dynamic Analyses. Constr. Build. Mater. 2020, 232, 117216.
49. Oliveira, D. V.; Silva, R.A.; Garbin, E.; Lourenço, P.B. Strengthening of Three-Leaf Stone Masonry Walls: An Experimental Research. Mater. Struct. 2012, 45, 1259–1276.
50. Milosevic, J.; Gago, A.S.; Lopes, M.; Bento, R. Experimental Assessment of Shear Strength Parameters on Rubble Stone Masonry Specimens. Constr. Build. Mater. 2013, 47, 1372–1380, doi:10.1016/j.conbuildmat.2013.06.036.
51. EN 1015-11 Methods of Test for Mortar for Masonry - Part 11: Determination of Flexural and Compressive Strength of Hardened Mortar; European Committee for Standardization, 2006; Vol. 3;.
52. TS EN ISO 6892-1 Metallic Materials — Tensile Testing — Part 1: Method of Test at Room Temperature; Turkish Standard, Ankara, 2016;
53. Demir, C. Seismic Behaviour of Historical Stone Masonry Multi-Leaf Walls, Doktora tezi, İstanbul Teknik Üniversitesi, Fen Bilimleri Enstitüsü, İstanbul, 2012.
54. Pluijm, R. van der Out-of-Plane Bending of Masonry : Behaviour and Strength, Doktora tezi, Eindhoven Teknoloji Üniversitesi, Eindhoven, 1999.
55. Liu, P.F.; Li, H.N.; Li, G.; Ansari, F.; Li, C. Out-of-Plane Seismic Behavior of Cast-in-Situ Composite Wall with Metal Tailing Porous Concrete. Eng. Struct. 2020, 210, 110346, doi:10.1016/j.engstruct.2020.110346.
56. Türkmen, S.; Wijte, S.N.M.; De Vries, B.T.; Ingham, J.M. Out-of-Plane Behavior of Clay Brick Masonry Walls Retrofitted with Flexible Deep Mounted CFRP Strips. Eng. Struct. 2021, 228, 111448, doi:10.1016/j.engstruct.2020.111448.
57. Buzov, A.; Radnić, J.; Grgić, N. Effects of Several Bolt Parameters on the Bearing Capacity of a Composite Multi-Drum Stone Column under an Earthquake. Compos. Part B Eng. 2019, 162, 250–258.
58. Petry, S.; Beyer, K. Scaling Unreinforced Masonry for Reduced-Scale Seismic Testing. Bull. Earthq. Eng. 2014, 12, 2557–2581, doi:10.1007/s10518-014-9605-1.
59. Silva, B.; Dalla Benetta, M.; Da Porto, F.; Modena, C. Experimental Assessment of In-Plane Behaviour of Three-Leaf Stone Masonry Walls. Constr. Build. Mater. 2014, 53, 149–161, doi:10.1016/j.conbuildmat.2013.11.084.
60. Parisi, F.; Balestrieri, C.; Asprone, D. Nonlinear Micromechanical Model for Tuff Stone Masonry: Experimental Validation and Performance Limit States. Constr. Build. Mater. 2016, 105, 165–175.
61. Guadagnuolo, M.; Aurilio, M.; Basile, A.; Faella, G. Modulus of Elasticity and Compressive Strength of Tuff Masonry: Results of a Wide Set of Flat-Jack Tests. Buildings 2020, 10.
62. Veríssimo-Anacleto, J.; Ludovico-Marques, M.; Neto, P. An Empirical Model for Compressive Strength of the Limestone Masonry Based on Number of Courses – An Experimental Study. Constr. Build. Mater. 2020, 258, 119508.
63. Garcia-Ramonda, L.; Pelá, L.; Roca, P.; Camata, G. In-Plane Shear Behaviour by Diagonal Compression Testing of Brick Masonry Walls Strengthened with Basalt and Steel Textile Reinforced Mortars. Constr. Build. Mater. 2020, 240, doi:10.1016/j.conbuildmat.2019.117905.
64. Harris, K.A.; Sharma, B. Nonconventional and Vernacular Construction Materials; 2016; ISBN 9781782423058.

 doi:10.20944/preprints202304.0444.v1

65. Binda, L.; Pina-Henriques, J.; Anzani, A.; Fontana, A.; Lourenço, P.B. A Contribution for the Understanding of Load-Transfer Mechanisms in Multi-Leaf Masonry Walls: Testing and Modelling. Eng. Struct. 2006, 28, 1132–1148.
66. Silva, R.A.; Oliveira, D. V.; Lourenço, P.B. On the Strengthening of Three-Leaf Stone Masonry Walls. In Proceedings of the Structural Analysis of Historic Construction: Preserving Safety and Significance; Taylor & Francis Group: London, 2008; pp. 739–746.
67. Milosevic, J.; Gago, A.S.; Lopes, M.; Bento, R. Experimental Assessment of Shear Strength Parameters on Rubble Stone Masonry Specimens. Constr. Build. Mater. 2013, 47, 1372–1380.